# Precision studies of the Higgs boson decay channel H→ZZ→4ℓ with MEKD

Paul Avery, Dimitri Bourilkov, Mingshui Chen, Tongguang Cheng, Alexey Drozdetskiy, James S. Gainer, Andrey Korytov, Konstantin T. Matchev, Predrag Milenovic, Guenakh Mitselmakher, Myeonghun Park, Aurelijus Rinkevicius, and Matthew Snowball

Phys. Rev. D **87**, 055006 — Published 8 March 2013

DOI: 10.1103/PhysRevD.87.055006

# Precision studies of the Higgs boson decay channel $H \to ZZ \to 4\ell$ with MEKD

Paul Avery,[1] Dimitri Bourilkov,[1] Mingshui Chen,[1] Tongguang Cheng,[1] Alexey Drozdetskiy,[1] James S. Gainer,[1,*] Andrey Korytov,[1] Konstantin T. Matchev,[1] Predrag Milenovic,[1] Guenakh Mitselmakher,[1] Myeonghun Park,[2] Aurelijus Rinkevicius,[1] and Matthew Snowball[1]

[1] *Physics Department, University of Florida, Gainesville, FL 32611, USA.*
[2] *CERN Physics Department, Theory Division, CH-1211 Geneva 23, Switzerland.*

(Dated: December 24, 2012)

The importance of the $H \to ZZ \to 4\ell$ "golden" channel was shown by its major role in the discovery, by the ATLAS and CMS collaborations, of a Higgs-like boson with mass near 125 GeV. We analyze the discrimination power of the matrix element method both for separating the signal from the irreducible ZZ background and for distinguishing various spin and parity hypotheses describing a signal in this channel. We show that the proper treatment of interference effects associated with permutations of identical leptons in the $4e$ and $4\mu$ final states plays an important role in achieving the best sensitivity in measuring the properties of the newly discovered boson. We provide a code, MEKD, that calculates kinematic discriminants based on the full leading order matrix elements and which will aid experimentalists and phenomenologists in their continuing studies of the $H \to ZZ \to 4\ell$ channel.

## CONTENTS

## I. INTRODUCTION

The CERN LHC collaborations recently reported the observation of a new bosonic particle with mass $m \sim 125$ GeV[1,2]. The production rates in the main discovery channels are consistent with the expectations for the Higgs boson, $H$, of the Standard Model (SM).

The most useful channels for the discovery of the Higgs-like boson and early measurements of its properties are $H \to \gamma\gamma$[3–5] and $H \to ZZ \to 4\ell$[6–9]. Each of these discovery channels has strengths and weaknesses. For example, observation of the appropriate excess in diphoton events immediately implies that the discovered resonance is not spin one[10,11]. At the same time, because of the much larger background, measuring the exact properties of the object in $\gamma\gamma$ events will be quite challenging[12–18].

In contrast, the "golden channel" $H \to ZZ \to 4\ell$[7] offers the opportunity for clean measurements of the mass, spin, parity, etc. of the new resonance in a controlled environment with low backgrounds. Furthermore, the four lepton final state allows experiments to probe the polarization of the intermediate $Z$ bosons through angular correlations. Thus, most of previous theoretical work on spin and parity discrimination has concentrated on this channel[12,16,19–37]; see also[38–42]. In fact, CMS and ATLAS have already shown that the interpretation of this resonance as CP odd is strongly disfavored, using information from this channel[8,9].

At the same time, relatively little theoretical effort has gone into using the kinematics of four leptons, besides their invariant mass, for discriminating between the Higgs signal and the SM background in this channel; see, however[6,7,30,31,43]. Discriminating between signal and background is an important issue, though, whether for determining the significance of the signal in this channel or for accurately measuring the spin and parity properties of the resonance. This is because for an SM Higgs boson with mass near 125 GeV, the rate of background events in comparison with that of the signal is not negligible; in fact, the signal to background ratio for a four lepton mass window of $\pm 2\sigma_{m_{4\ell}}$ is roughly 2:1[8,9]. (Here, $\sigma_{m_{4\ell}}$ stands for the experimental four lepton mass resolution.)

Another motivation for revisiting the previous work on this channel is that much of the previous literature is limited to the case of a heavy Higgs boson, with mass above the $ZZ$ threshold, where both $Z$ bosons produced in the Higgs decay will be on-shell. Most previous studies of this channel in the low Higgs boson mass range have lacked diagrams involving permutations of identical leptons, and hence the associated interference, in the $4e$ and $4\mu$ final states. Such permutations are relatively unimportant when both $Z$ bosons are mostly on-shell. However, as we show in this paper, the inclusion of these interference effects plays an important role in achieving the best possible sensitivities in the low mass range and is crucially important for separating spin zero and spin two resonance hypotheses.

One of the great advantages of the golden channel is that the final state is fully reconstructed and well-measured. However, the presence of four leptons in the final state means that, at leading order, there are eight independent observed degrees of freedom (in the Higgs CM frame), not counting the irrelevant azimuthal orientation of the event. The existence of eight meaningful kinematic variables strongly motivates the use of a Multivariate Analysis (MVA)[44] technique, and in particular the Matrix Element Method (MEM)[16,30,31,43,45–47], thereby allowing all of the information in each event to be used in either distinguishing signal from background or in distinguishing between different signal spin/parity hypotheses. Both the MEM and other MVA approaches presumably achieve an approximately identical level of discrimination. However, the MEM has several advantages over other MVAs. The quantity used in the MEM analysis is the (squared) matrix element, which is (up to approximations used) uniquely defined from first principles, while MVA-based discriminants require an ad hoc training on very large Monte Carlo samples. Since the matrix element has a clear, well-understood physical meaning, one is able to make a direct connection between the features of a statistical analysis and the underlying physics. This is particularly true in the case of the golden channel, as the distributions of kinematic variables can be determined from the amplitudes for producing $Z$ bosons with given helicities[48,49].

In contrast with even the recent past, there are now a number of commonly used and well-tested programs which can be utilized to calculate matrix elements automatically[50]. These include tools to generate model files from an arbitrary Lagrangian, such as FeynRules[51] and LanHEP[52], as well as tools to calculate the matrix elements using these model files, such as MadGraph[53,54], CalcHEP[55], and CompHEP[56,57]. Taken together, these tools allow for relatively automatic implementation of new models and automatic generation of matrix elements, as explained at the TASI-2011 summer school[58] and the MC4BSM-2012 workshop[50,59]. The existence of such tools considerably simplifies calculations of leading order matrix elements for any desired process and strongly motivates the use of the MEM where possible. It is this approach that we take in the presented paper.

In Sec. II, we review the MEM and describe the associated variable, the kinematic discriminant $KD$, which quantifies the extent to which a particular event is described by one hypothesis as opposed to another. We also show the superiority of the MEM over analyses involving fewer variables. Next, we calculate $KD$ for signal and background events using different tools: MadGraph[54] in Sec. III, and CalcHEP[55] and NLOME[60,61] in Appendix A. In Sec. IV we compare the results for the kinematic discriminant computed with these three tools and show that they are in agreement. We also analyze the relevance of interference in the $4e$ and $4\mu$ final states in the context of SM Higgs boson

signal vs. background separation. In Sec. V, we discuss the added benefit from incorporating experimentally-known information about the initial state into the analysis. Sec. VI quantifies the effect of the spin and CP of the resonance on the ability to separate signal from background.

In Sec. VII we demonstrate the application of the MEM to discrimination between different spin/parity signal hypotheses. We show that properly taking into account the above-mentioned interference effects in the $4e$ and $4\mu$ final states significantly enhances the separation power between alternative signal hypotheses. Sec. VIII summarizes our findings and outlines directions for future work. The notation for the relevant kinematic variables in the Higgs golden channel are given in Appendix B.

In order to facilitate future MEM-based studies of the properties of the newly discovered four lepton resonance by the experimental and theoretical communities, we are making public one of the two new $KD$ codes used in this paper (the MadGraph-based code, which we call MEKD). The instructions on how to install and run the code are given in Appendix C. This code calculates matrix elements and kinematic discriminants, natively including diagrams with swapped identical leptons (and the associated interference) in the $4e$ and $4\mu$ final states, background diagrams with $\gamma^*$ propagators for the "doubly resonant" $q\bar{q} \to ZZ \to 4\ell$ process and singly resonant $q\bar{q} \to Z \to 4\ell$ production[62]. It does not use a narrow width approximation for either the $Z$ bosons or the signal resonance.

## II. PRELIMINARIES

We now define the MEM and note some modifications to the general procedure which are useful in studying the golden channel. We then describe a practical method for displaying the sensitivity of different kinematic discriminants. Finally, we demonstrate the increase in discrimination power that may be obtained using the MEM, in comparison with analyses which use fewer variables.

### A. The matrix element method and its kinematic discriminant $KD$

For a four lepton event described by kinematic information $\mathbf{p}$, the best possible discriminant between two production hypotheses $A$ (e.g. signal) and $B$ (e.g. background), is the ratio of the probabilities to observe such an event, given the alternative production hypotheses:

$$D(A;B) = \frac{P(\mathbf{p}\,|\,A)}{P(\mathbf{p}\,|\,B)}. \tag{1}$$

Here, $P(\mathbf{p}\,|\,A)$ and $P(\mathbf{p}\,|\,B)$ are the probability density functions (*pdf*s) for observing the event in the cases of hypotheses $A$ and $B$, respectively. Note that the alternative definition of the discriminant $\tilde{D}$:

$$\tilde{D}(A;B) = \frac{\alpha\, P(\mathbf{p}\,|A) + \beta\, P(\mathbf{p}\,|B)}{P(\mathbf{p}\,|\,B)}, \tag{2}$$

may seem to be more suited for the case when the alternative hypotheses are *signal+background* or *background-only*. However, $\tilde{D}$ is a monotonic function of $D$ and, hence, considering $\tilde{D}$ rather than $D$ does not add or subtract any information.

In particle physics, probabilities $P(\mathbf{p})$ can be represented by the differential cross section of a signal or background process with respect to the variables considered, $d\sigma/d\mathbf{p}$, scaled by the instrumental efficiencies $\epsilon(\mathbf{p})$, and normalized by the appropriate total cross section within the instrumental acceptance:

$$P(\mathbf{p}) = \frac{d\sigma/d\mathbf{p}\ \epsilon(\mathbf{p})}{\int d\sigma/d\mathbf{p}\ \epsilon(\mathbf{p})\ d\mathbf{p}}. \tag{3}$$

Following the same logic of comparing discriminants $D$ and $\tilde{D}$, one can see that the normalization constants in the definitions of $P(\mathbf{p})$ do not matter and can be dropped; the instrumental efficiencies appearing in the numerator and denominator cancel out; and one arrives at the following definition of the kinematic discriminant between two chosen processes A and B, e.g. signal and background:

$$KD(A;\,B) = \ln\left(\frac{d\sigma_A/d\mathbf{p}}{d\sigma_B/d\mathbf{p}}\right). \tag{4}$$

We use log of the ratio only for technical convenience; this is dictated by the large dynamic range in the ratio of cross sections involved. If all signal and background processes involve effectively massless initial state partons (as is often the case), the phase space factors are identical for all processes and hence cancel in the ratio. Thus, we find that

$$KD(A;B) = \ln\left(\frac{\sum\limits_{a,b} f_a(x_1)\cdot f_b(x_2)\cdot\left|\mathcal{M}_A(a+b\to 4\ell)\right|^2}{\sum\limits_{a',b'} f_{a'}(x_1)\cdot f_{b'}(x_2)\cdot\left|\mathcal{M}_B(a'+b'\to 4\ell)\right|^2}\right). \tag{5}$$

In this equation, $a$ and $b$ ($a'$ and $b'$) stand for different types of partons which can produce the four lepton final state via process A (B) with corresponding matrix elements $\mathcal{M}_A$ ( $\mathcal{M}_B$). The momenta of the partons are fully defined by the final state and are denoted by $x_1$ and $x_2$ in units of the initial proton energy. The functions $f(x)$ are the parton distribution functions (PDFs), with the subscripts indicating which types of partons they correspond to.

The products of PDFs in the numerator and denominator of Eq. (5) in general do not cancel. In particular they do not cancel if hypothesis $A$ is $gg\to H\to ZZ\to 4\ell$ and hypothesis $B$ is $q\bar{q}\to ZZ^*\to 4\ell$. Note that Eq. (5) is invariant under any changes of variables, as any resulting Jacobian would be common to both the signal and background expressions and hence would cancel in the ratio.

One may wish to ignore the information related to the momentum distribution of the initial state partons inside the proton and effectively consider only the information encoded in the decay itself. Then the kinematic discriminant (5) simplifies to become:

$$KD(A;B) = \ln\left(\frac{\left|\mathcal{M}_A(a+b\to 4\ell)\right|^2}{\left|\mathcal{M}_B(a'+b'\to 4\ell)\right|^2}\right). \tag{6}$$

In Sec. V, we explicitly analyze whether this simplification results in a substantial loss in our ability to discriminate signal from background.

There is an experimental complication that we have ignored so far, namely that the momenta of the final state leptons are not perfectly measured. Generally, one can take this into account by including an integration over transfer functions for the final state momenta in both the numerator and denominator of Eqs. (5) or (6); these integrals do not cancel in the ratio. The transfer functions would need to include parameterizations of momentum mismeasurements and reconstruction efficiencies in the entire phase space relevant for the analysis. Since leptons are well-measured, one can use delta function transfer functions for many applications involving leptons in the final state. However, in the case in which the signal process is the production of a narrow resonance, the value of the signal matrix element will be very sensitive to small perturbations in the measured invariant mass when the instrumental mass resolution is similar to or greater than the resonance width. This is the case for the channel we consider; the width of a 125 GeV SM Higgs boson is only about 4 MeV[63], while the instrumental four lepton mass resolution is in neighborhood of 1 GeV[6–9]. To avoid complications associated with using transfer functions, we employ the approach used in the CMS $H\to ZZ^*\to 4\ell$ analyses[7,8]. In this approach, the four lepton mass information is factorized from the rest of the kinematic information by calculating the signal matrix element for $m_H = m_{4\ell}^{obs}$, where $m_{4\ell}^{obs}$ is the observed four lepton mass of a given event:

$$\left|\mathcal{M}_H(a+b\to 4\ell)\right|^2 = \left|\mathcal{M}_H(gg\to H\to 4\ell\,|\,m_H = m_{4\ell}^{obs})\right|^2, \tag{7}$$

This matrix element can be used both in Eqs. (5) and (6). The instrumental four lepton mass resolution is then encoded in 2D-*pdf*'s:

- for signal: $pdf_H(m_{4\ell}, KD\,|\,m_H) = pdf_H(m_{4\ell}\,|\,m_H)\cdot pdf_H(KD\,|\,m_{4\ell})$;
- for background: $pdf_{ZZ}(m_{4\ell}, KD) = pdf_{ZZ}(m_{4\ell})\cdot pdf_{ZZ}(KD\,|\,m_{4\ell})$,

which are ultimately used for the construction of the test statistic itself.

### B. Event generation

For the analyses described below, we use parton-level events generated with MadGraph[54,64,65]. Both signal and background events were generated within the four lepton mass window $120 < m_{4\ell} < 130$ GeV. When generating the signal, we use a nominal Higgs boson mass of $m_H = 125$ GeV. For background $ZZ$ events, only processes initiated by the first two generation quarks were generated. The lepton acceptance cuts were[8]

- $p_T > 7$ GeV and $|\eta| < 2.5$ for electrons,
- $p_T > 5$ GeV and $|\eta| < 2.4$ for muons.

Events are generated for each possible choice of final state flavors, namely $e^-e^+\mu^-\mu^+$ ("different favor", DF), and $e^-e^+e^-e^+$ and $\mu^-\mu^+\mu^-\mu^+$ ("same flavor", SF). In the case of DF events, opposite-charge lepton pairs are formed by flavor $(e^-e^+)(\mu^-\mu^+)$. In the SF case, two different pairings of opposite-charge leptons are possible, e.g. $(e_1^-e_2^+)(e_3^-e_4^+)$ and $(e_1^-e_4^+)(e_3^-e_2^+)$. The invariant mass of a pair closest to the mass of Z boson is $m_{Z1}$ ($m_{12}$) in CMS (ATLAS) notations, while the invariant mass of the other pair is $m_{Z2}$ ($m_{34}$). We accept the event if at least one pairing of leptons passes the invariant mass cuts of 40 and 12 GeV on $m_{Z1}$ ($m_{12}$) and $m_{Z2}$ ($m_{34}$), respectively. We do not perform any detector simulation as our primary concern is with the comparison of the different analyses as opposed to the absolute performance of any given analysis.

### C. ROC curves

We wish to characterize the extent to which our $KD$ is useful in enhancing the sensitivity of an analysis. One can generate pseudoexperiments using the two-dimensional *pdf*s (involving KD and invariant mass $m_{4\ell}$) described above and perform a statistical analysis on how well two hypotheses can be separated. In fact, we perform such a prototypical analysis in Sec. VII. However, a simpler and more intuitive means of displaying the extent to which signal and background may be separated is provided by "Receiver Operating Characteristic" (ROC) curves[66].

Using generated events (see previous subsection), we build distributions of $KD(A;B)$ for processes A and B that we wish to compare. Then, we calculate cumulative probabilities $\epsilon_A(\,KD \geq KD_{\rm CUT}\,)$ and $\epsilon_B(\,KD \geq KD_{\rm CUT}\,)$. The plot of $\epsilon_A(\,KD \geq KD_{\rm CUT})$ versus $\epsilon_B(\,KD \geq KD_{\rm CUT})$, as one smoothly increases the cut value $KD_{\rm CUT}$, is the ROC curve. The curve gives the fraction of process A events that pass a given cut on $KD$ in terms of the fraction of process B events passing the same given cut. The further the curve is from the diagonal ($\epsilon_A = \epsilon_B$), the better the cut has separated the two processes.

### D. Comparison with single variable analyses

The most sensitive kinematic variable for distinguishing signal and background is, of course, the invariant mass of the event. However, if we want to move beyond this and obtain greater sensitivity, a natural question is whether we truly need to use all of the kinematic variables in our analysis, or whether using one or two particularly sensitive variables would suffice. We therefore investigate the angular variables $\theta^*$ and $\Phi$, in the convention of Refs.[16,30], as well as $m_{Z2}$, the mass of the less massive opposite-charge dilepton pair[67]. We choose $m_{Z2}$ in particular, as due to the $Z\gamma^*$ contribution to the background, the signal and background shapes are significantly different. The $ZZ$ background has a substantial fraction of events with $m_{Z2}$ values close to the cut value of 12 GeV, while for a Higgs boson decaying to actual $Z$ bosons at tree level, the low values of $m_{Z2}$ are substantially less likely (due to the loop suppression, the $H \to Z\gamma^*$ decay can be neglected). The motivation for considering the angle $\theta^*$, which is the $Z$ boson polar angle in the center of mass frame of the event, is that the background $\theta^*$ distribution is much more peaked in the forward and backward directions (in comparison with signal). This is due to the $t$-channel nature of the $q\bar{q} \to ZZ$ processes. The angle $\Phi$, the angle between the two dilepton decay planes, has often been considered in the literature for distinguishing between spin and parity hypotheses (see, e.g., Refs.[19,23]).

Using simulated SM Higgs boson and $ZZ$ background events, we construct numerical *pdf*s $P_s(x)$ and $P_b(x)$ for each of these variables (here $x$ stands for either $m_{Z2}$ or $\theta^*$ or $\Phi$). We then take the ratio of these probabilities to construct discriminants and produce corresponding ROC curves. These three ROC curves are shown in Fig. 1, along with the ROC curve constructed using the MEM $KD(H;ZZ)$ calculated using the MadGraph matrix element (see Sec. III for details). One can see that the analysis utilizing $KD(H;ZZ)$ based on the complete matrix element is the most sensitive. We also note that $m_{Z2}$ is very sensitive in its own right. This observation will become important in Sec. VI, where we discuss the signal vs. background separation when assuming different signal hypotheses.

### E. Overview of available tools for calculating $KD$

Since an event generator performs a Monte Carlo integration of a matrix element squared over the relevant phase space, in principle *any* event generator can be used to calculate the matrix element, given the final state kinematics. Unfortunately, not all event generators have implemented this functionality.

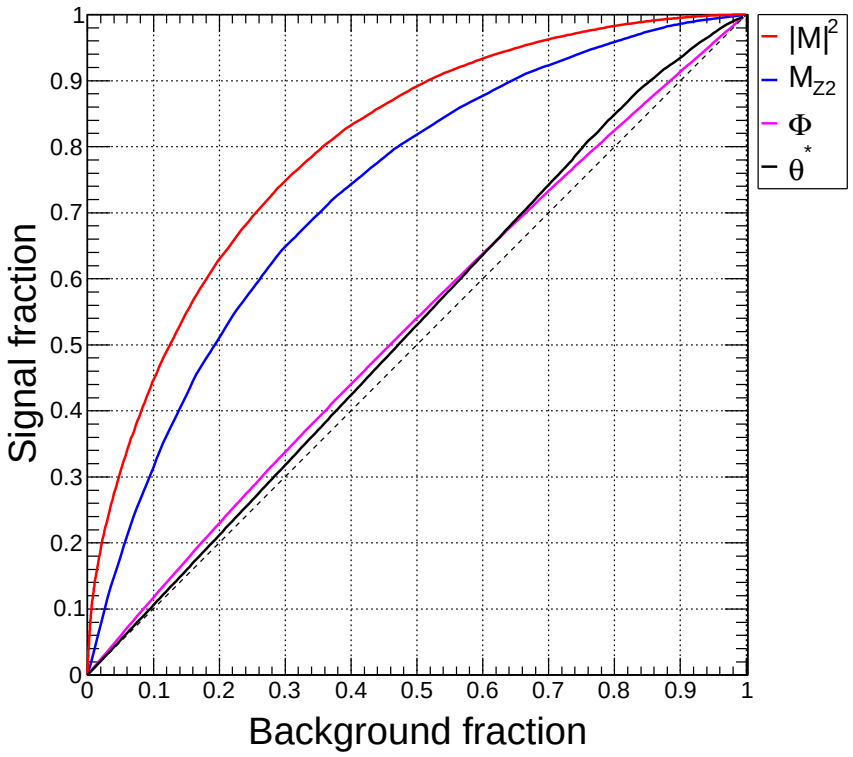


FIG. 1. Comparison of different ROC curves based on: the value of $KD$ obtained from matrix elements (red curve), $m_{Z2}$ (blue curve), $\Phi$ (magenta curve), and $\theta^*$ (black curve). The black dashed diagonal line is the ROC curve obtained from cutting events indiscriminately (e.g., by flipping a fair coin or by only considering some fraction of the data set).

In this paper, we shall use MadGraph[53,54], and CalcHEP[55], which can easily provide analytical expressions for the matrix element for the relevant $2 \to 4$ scattering processes, e.g, $gg \to H \to ZZ^* \to 4\ell$ for signal and $q\bar{q} \to ZZ^* \to 4\ell$ for the background. MadGraph and CalcHEP are on a relatively equal footing — they are both highly automated and very flexible, and thus provide a useful cross-check on each other (this test is performed in Appendix A). Using the built-in flexibility of these generators, we construct a higher-level package, MEKD (Sec. III), that calculates complete leading order matrix elements for $gg \to X \to 4\ell$ and $q\bar{q} \to 4\ell$ for any given four lepton final state. This package was used along with the MELA package, to be described below, by CMS in their most recent update on the observation of the newly discovered boson decaying to $ZZ \to 4\ell$ and the measurements of its properties in this channel[8].

As an alternative to the automated tools, one could utilize a specialized package, perhaps because it has the expressions for the relevant matrix elements readily available or because it offers extra functionality not accessible in the automated tools. Two examples of this type include NLOME[7661], which is based on the MCFM event generator[60], and JHUGen[68]. The crucial advantage of NLOME over all other competitors is its next-to-leading order (NLO) functionality[45,46]. On the other hand, the $H \to ZZ \to 4\ell$ channel is built around the matrix element for the DF $e^-e^+\mu^-\mu^+$ final state. Therefore, when applying it to events with the SF $4e$ or $4\mu$ final states, the interference effects are missed. Also, signals of alternative spins and parities are not available in this package. JHUGen allows one to extract the leading order matrix element for a broad spectrum of possible signal hypotheses, but does not calculate the matrix element for backgrounds.

There is yet another option: one may wish to code one's own software package using expressions for matrix elements found in the literature, such as those in Ref.[16,30] for signal and Ref.[43,47] for background. This approach was used by both CMS and ATLAS. Although the corresponding software packages used by the two experiments are not publicly available, for completeness we describe their main features, derived from the references the codes are based on.

In their new boson discovery paper[7], the CMS collaboration used the MELA package which is largely based on the work in[16,30]. For an event with four lepton mass $m_{4\ell}$ above the on-shell ZZ threshold, the signal and background probabilities for the event, $P_{\rm H}(\,\mathbf{\Omega}\,|\,m_{\rm H} = m_{4\ell}\,)$ and $P_{\rm ZZ}(\,\mathbf{\Omega}\,|\,m_{4\ell}\,)$, were calculated analytically using equations from

Refs.[30,43]. Here, the vector $\mathbf{\Omega}$ denotes five angles describing the four lepton system in its center of mass frame (see Appendix B). For an event with four lepton mass below the on-shell ZZ threshold, the dilepton masses $m_{Z1}$ and $m_{Z2}$ must be included in the matrix element calculations. The signal probability $P_{\rm H}(\,m_{Z1},m_{Z2},\mathbf{\Omega}\,|\,m_{\rm H}=m_{4\ell}\,)$ was calculated analytically[16], while the background probability was tabulated from template distributions for $m_{Z1}$, $m_{Z2}$, and the five angles, obtained with the POWHEG simulation at generator level[7,69]. The analytic computations of the matrix elements did not include same-type lepton permutations and associated interferences effects in the SF four lepton final states.

In the recently released $H\to ZZ\to 4\ell$ analysis update by CMS[8], the MELA package was upgraded and now includes the background probability $P_{\rm ZZ}(\,m_{Z1},m_{Z2},\mathbf{\Omega}\,|\,m_{4\ell}\,)$ for the low mass range calculated analytically using parameterizations from Ref.[47]. The permutation/interference effects for the SF four lepton final states are still ignored. In the same Ref.[8], CMS also used the MEKD package, which has complete leading order matrix elements for signal and background, including the proper treatment of lepton permutations and the associated interference present in SF four lepton final states.

In their recent update on the $H\to ZZ\to 4\ell$ channel[9], ATLAS also used the matrix element method for testing various spin-parity hypotheses for the newly discovered boson. In these analyses, the kinematic discriminants are built solely from signal matrix elements based on Ref.[16]. Hence, the constructed kinematic discriminants do not account for permutations of identical leptons and the associated interference. Ignoring the presence of background in these MEM-based analyses also makes them even less optimal.

Given that the permutation/interference effects have not always been consistently implemented in the past, a large part of the results and discussion presented below are focused on the investigation of the effects from interference on the physics results. We show that in some cases the interference effects play a significant role and should not be neglected in separating alternative hypotheses describing the observed excess of events near the mass of 125 GeV.

## III. MATRIX ELEMENT KINEMATIC DISCRIMINANT (MEKD)

The MEKD code is a publicly available package[70]; the instructions for download and usage are provided in Appendix C. This code uses MadGraph to calculate complete LO matrix elements for signal $gg\to X\to ZZ\to 4\ell$ and background process $q\bar{q}\to ZZ\to 4\ell$ and also builds the kinematic discriminants according to Eqs. (5) and (6). The SM Lagrangian and the non-SM additions are implemented automatically into MadGraph via FeynRules[51].

The MEKD calculations are validated twice: first, by comparing matrix elements calculated by MadGraph and CalcHEP, both embedded into the same MEKD framework; and, second, by comparing the matrix elements calculated within the MEKD framework with the LO matrix elements calculated by the standalone NLOME package. The MadGraph vs. CalcHEP validation is performed for all three final states, $4e$, $4\mu$, $2e2\mu$, separately, while MadGraph vs. NLOME validation is performed only for the $2e2\mu$ final state (the version of NLOME available to us did not include interference for the $4e$ and $4\mu$ final states). The results are found to be identical for all practical purposes; the details can be found in Appendix A.

In the current version of MEKD, the SM Lagrangian is extended to allow for non-SM couplings of a spin zero or spin two resonance to gluons and to $Z$ bosons. To be specific, following[16,30], we implement the following terms in the Lagrangian for a spin zero resonance:

$$\mathcal{L}_{HZZ}\ni -\frac{g_{1z}}{2}HZ_\mu Z^\mu-\frac{g_{2z}}{4}HZ_{\mu\nu}Z^{\mu\nu}-\frac{g_{3z}}{2}Z_{\mu\alpha}Z^{\mu\beta}\left(\partial_\beta\,\partial^\alpha H\right)-\frac{g_{4z}}{4}HZ_{\mu\nu}\tilde{Z}^{\mu\nu}, \tag{8}$$

$$\mathcal{L}_{Hgg}\ni -\frac{g_{1g}}{2}HF^a_\mu F^{a,\mu}-\frac{g_{2g}}{4}HF^a_{\mu\nu}F^{a,\mu\nu}-\frac{g_{3g}}{2}F^a_{\mu\alpha}F^{a,\mu\beta}\left(\partial_\beta\,\partial^\alpha H\right)-\frac{g_{4g}}{4}HF^a_{\mu\nu}\tilde{F}^{a,\mu\nu}, \tag{9}$$

where $H$ is generic scalar field, $Z(F)^\mu$ is the vector potential for the $Z$ boson (gluon), and $Z(F)^{\mu\nu}$ is the field strength tensor for the $Z$ boson (gluon). For the specific case of the SM Higgs boson, one has

$$(g_{1z},g_{2z},g_{3z},g_{4z})=\left(\frac{2m_Z^2}{<v>},0,0,0\right), \tag{10}$$

$$(g_{1g},g_{2g},g_{3g},g_{4g})=(0,g_{\rm eff,0,0})\,. \tag{11}$$

Another hypothesis which we will consider below is a CP odd spin zero resonance, for which we have

$$(g_{1z},g_{2z},g_{3z},g_{4z})=\left(0,0,0,g'_{\rm eff,Z}\right), \tag{12}$$

$$(g_{1g},g_{2g},g_{3g},g_{4g})=\left(0,0,0,g'_{\rm eff,g}\right), \tag{13}$$

where the product of $g'_{\rm eff,Z}$ and $g'_{\rm eff,g}$ is chosen so that we obtain the same total cross section times branching ratio as in the case of the SM Higgs boson. Of course, for a spin zero resonance, no angular distributions depend on which particular couplings with gluons are non-vanishing, at least at leading order.

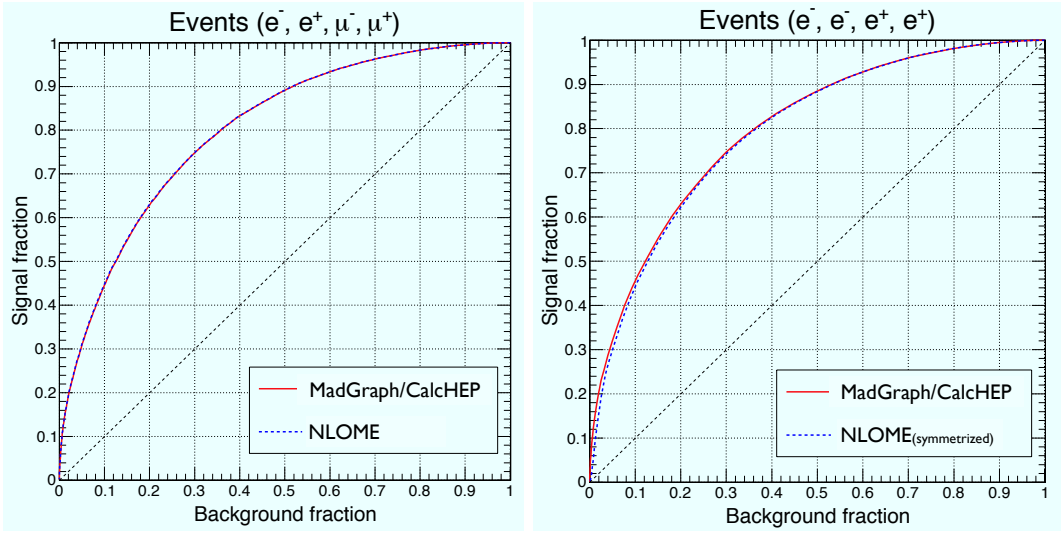


FIG. 2. Comparison of ROC curves obtained from the different implementations of the kinematic discriminant: from MadGraph/CalcHEP (red solid lines) or from NLOME (blue dotted lines), for DF (left) and SF (right) $4\ell$ events.

In the case of a general spin two resonance, we have

$$\begin{aligned}\mathcal{L}_{GZZ} \ \ni & k_{1z} h_{\mu\nu} Z^{\mu\alpha} Z_{\alpha}^{\nu} + k_{2z} \left(\partial_\alpha \partial_\beta h_{\mu\nu}\right) Z^{\mu\alpha} Z^{\nu\beta} + k_{3z} h_{\beta\nu} \left(\partial^\alpha Z^{\mu\nu} \partial^\beta Z_{\mu\alpha} + \partial^\alpha Z_{\mu\alpha} \partial^\beta Z^{\mu\nu}\right) \\ & + k_{4z} h_{\mu\nu} \partial^\mu Z^{\alpha\beta} \partial^\nu Z_{\alpha\beta} + k_{5z} h_{\mu\nu} Z^\mu Z^\nu + k_{6z} (\partial_\alpha h_{\mu\nu}) Z^\nu \partial^\mu Z^\alpha + k_{7z} h_{\mu\nu} \partial^\mu Z^\alpha \partial^\nu Z_\alpha \\ & + k_{8z} h_{\mu\nu} \partial^\mu Z^{\alpha\beta} \partial^\nu \tilde{Z}_{\alpha\beta} + k_{9z} (\partial_\alpha h_{\mu\alpha}) \epsilon^{\mu\nu\rho\sigma} \left(\partial^\alpha Z_\nu\right) Z_\rho \\ & + k_{10z} \left(\partial_\beta \partial_\rho h_{\mu\alpha}\right) \epsilon^{\mu\nu\rho\sigma} \left(\partial^\alpha Z_\nu \partial_\sigma Z^\beta + \partial^\alpha Z^\beta \partial_\sigma Z_\nu\right), \end{aligned} \tag{14}$$

and an analogous effective Lagrangian $\mathcal{L}_{Ggg}$ describing the coupling of an arbitrary spin two resonance to gluons.

In what follows we will consider the hypothesis of a massive graviton[71], for which the values of couplings are

$$(k_{1z}, k_{2z}, k_{3z}, k_{4z}, k_{5z}, k_{6z}, k_{7z}, k_{8z}, k_{9z}, k_{10z}) = \left(k_{1z}, 0, 0, 0, -m_Z^2 k_{1z}, 0, 0, 0, 0, 0\right), \tag{15}$$

$$(k_{1g}, k_{2g}, k_{3g}, k_{4g}, k_{5g}, k_{6g}, k_{7g}, k_{8g}, k_{9g}, k_{10g}) = (k_{1g}, 0, 0, 0, 0, 0, 0, 0, 0, 0), \tag{16}$$

(see e.g. Ref.[72]), with the $k_{1z}$ and $k_{1g}$ set to give the same total cross section as in the SM Higgs boson case.

The user has complete freedom to adjust any of the couplings in the spin zero and spin two Lagrangians described above. The case of a spin one boson and other extended functionality are coming shortly. Hence, the MEKD code can be used for general studies of the Higgs-like resonance, and in particular for the measurement of these couplings[73].

## IV. SEPARATION OF THE STANDARD MODEL HIGGS BOSON AND BACKGROUND

As discussed in Sec. II C, the effectiveness of a kinematic discriminant can be assessed using the corresponding ROC curve. Figure 2 shows ROC curves characterizing the performance of the kinematic discriminant $KD(H; ZZ)$ that is built to sort events based on whether they are more likely to be produced via the SM Higgs boson or by $ZZ$ background processes. As shown in Appendix A, MadGraph and CalcHEP give identical results, so for the purposes of this figure we refer to them as MadGraph/CalcHEP.

Fig. 2 (left) shows that the ROC curves for $KD(H; ZZ)$ as obtained with NLOME and MadGraph/CalcHEP for $2e2\mu$ events are *identical*, as expected from the comparisons in Appendix A. One can see that if one were to use a simple cut on $KD$ as a part of the event selection in a SM Higgs boson search analysis, then one could suppress background by about a factor of two, while keeping 90% of signal events.

Fig. 2 (right) shows that the power of the kinematic discriminant to separate signal from background in the SF four lepton final states is approximately the same. However, a closer look shows a very small difference, $\mathcal{O}(1\%)$, between MadGraph/CalcHEP and NLOME(MCFM) results. This is due to the fact that NLOME(MCFM) is missing permutations of identical leptons and the associated interference present for SF four lepton final states. To alleviate the problem somewhat, we recycle the DF matrix element

$$\left|\mathcal{M}_{DF}\left((e^- e^+)(\mu^- \mu^+)\right)\right|^2$$

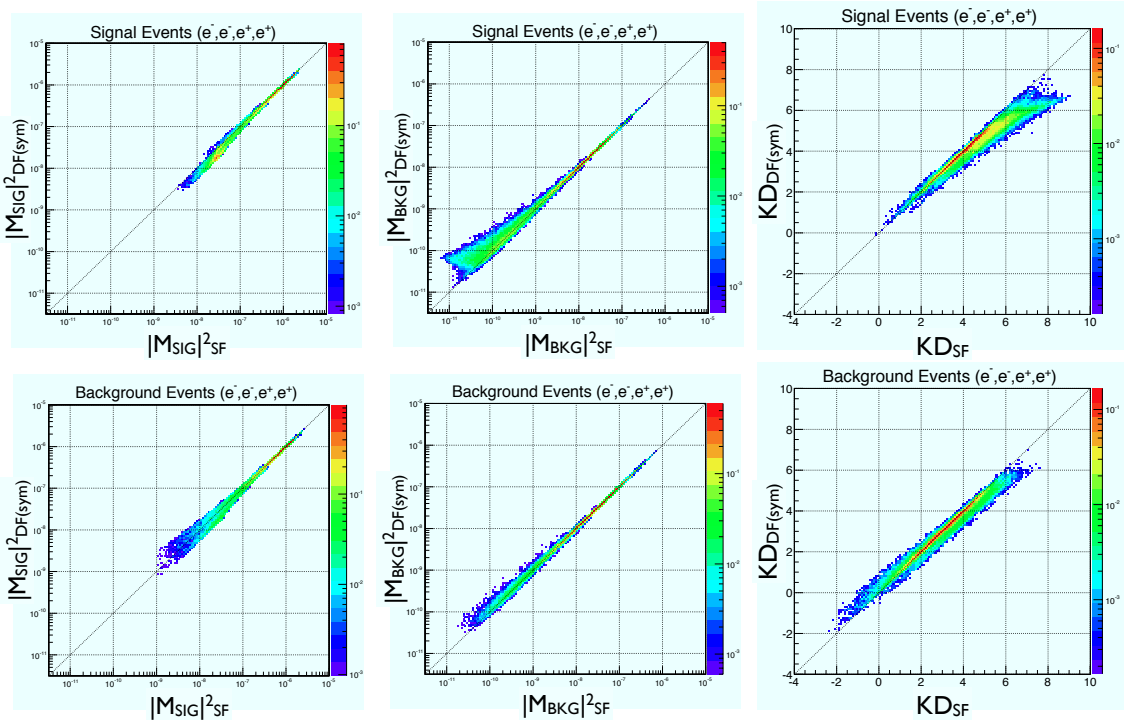


FIG. 3. Comparison of the signal (left column) and background (middle column) matrix elements, as well as the kinematic discriminant $KD_{\rm MAD}$ (right column), for signal events (top row) and background events (bottom row) as calculated with the full matrix element for SF events $|\mathcal{M}|^2_{SF}$ (including the interference) versus the approximation $|\mathcal{M}|^2_{DF(sym)}$ obtained by the patch given in Eq. (17). All quantities are calculated with MadGraph.

to make a "symmetrized" matrix element for the SF four lepton final states:

$$\left|\mathcal{M}_{SF}\left(e_1^- e_2^+ e_3^- e_4^+\right)\right|^2_{\rm symmetrized} \approx \left|\mathcal{M}_{DF}\left((e_1^- e_2^+)(e_3^- e_4^+)\right)\right|^2 + \left|\mathcal{M}_{DF}\left((e_1^- e_4^+)(e_3^- e_2^+)\right)\right|^2 , \tag{17}$$

which now includes permutations of identical leptons, but, of course, still misses the interference terms.

The effect of neglecting interference is more visible in Fig. 3, where we compare three quantities: $|\mathcal{M}_{\rm H}|^2$ (left column), $|\mathcal{M}_{\rm ZZ}|^2$ (middle column), and $KD(H;ZZ)$ (right column), all calculated in two different ways using MadGraph. The $x$ axis shows the full results for the SF final state. The $y$ axis shows the results obtained using the patch shown in Eq. (17). Since we use the exact same code, the only difference between $x$ and $y$ values is whether or not the interference contributions are taken into account in the corresponding code. Fig. 3 shows a fair amount of scatter for the matrix elements themselves as well as for their ratio; this explicitly shows the role of interference.

For the matrix elements, the scatter becomes noticeably worse for low values of the squared matrix element. This can be easily understood: for SF events, there are two amplitudes corresponding to the two ways of pairing the final state leptons. Normally, one pairing has one $Z$ on-shell and the other $Z$ off-shell, while the other pairing has both $Z$s off-shell. The result is then dominated by the on-shell amplitude squared and the interference terms are negligible. In order for the interference terms to become noticeable, both pairings should have *two* off-shell $Z$s in which case the overall matrix element squared will be small. We can easily observe this effect, especially for the background matrix element (the middle plots in the figure), for which the $Z\gamma^*$ amplitude is large, which more easily allows the $Z$s to be off-shell. The larger spread at low $|\mathcal{M}_{BKG}|^2$ appears at high $KD$ (right column plots), since the $KD$ ratio is inversely proportional to $|\mathcal{M}_{BKG}|^2$.

The reason why the obvious scatter seen in Fig. 3 has relatively little effect on the ROC curve in Fig. 2 (right) is easy to understand. The observed scatter (up to $\pm 0.5$ units of $KD$) is substantially smaller than the typical range of $KD$ values (about 4 units). Therefore, using the "incorrect" $KD$ does not significantly broaden the signal and background $KD$ distributions, and the signal vs. background separation power is not affected too much. The similarity of the left and right plots for DF and SF four lepton events in Fig. 2 is yet another sign that the relative role of interference effects is not expected to be large in separating signal and background. As we discuss in Sec. VII, this is not the case when separating alternative signal hypotheses.

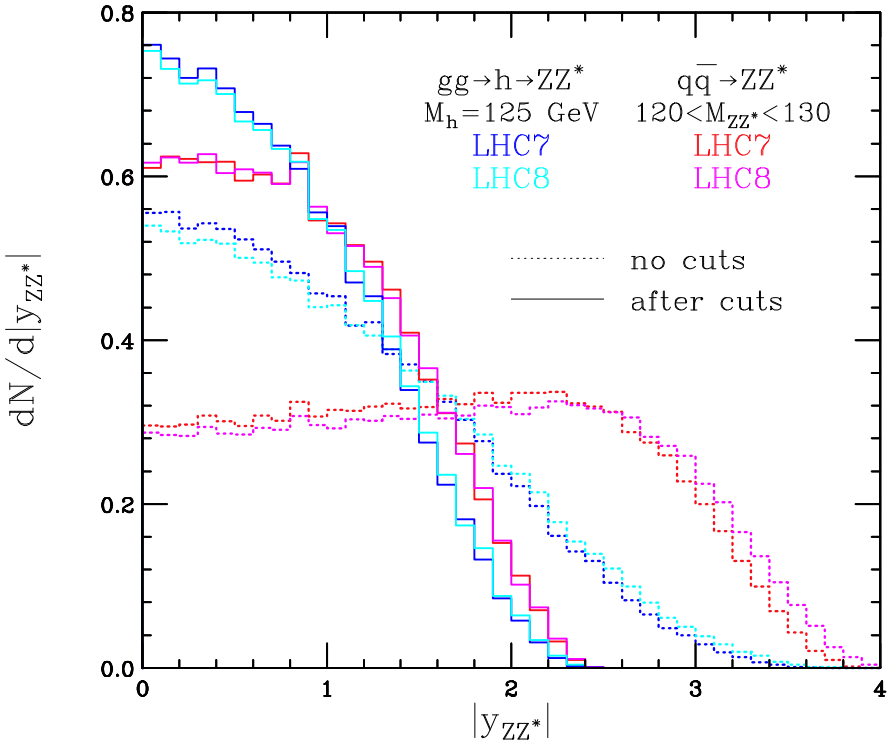


FIG. 4. Unit-normalized rapidity distributions of $ZZ^*$ events for signal (bluish colors) and background (reddish colors). Results are shown for two different LHC energies (7 and 8 TeV), before cuts (dashed lines) and after cuts (solid lines).

## V. INCLUDING INFORMATION ABOUT THE INITIAL STATE

In the Higgs golden channel, the final state is fully reconstructed and thus the momenta of the initial state partons may be inferred. In our discussion thus far, we have ignored this additional information, so a very relevant question is how much does one gain from considering it. To illustrate the idea, in Fig. 4 we plot the rapidity distributions for signal and background events generated with PYTHIA[74] at the two relevant LHC energies. The dashed histograms represent parton-level distributions before cuts. There is a substantial difference in the shapes of the signal and the background — the $Z$ bosons in the background events are much more forward, because they are produced from an asymmetric $q\bar{q}$ state, where typically the quark carries a larger momentum fraction. In contrast, the signal distributions are much more central, since the Higgs boson is produced from a symmetric $gg$ initial state, where the gluons are likely to share the momentum more evenly.

However, these large differences in the event rapidity distributions wash out in the presence of cuts (solid histograms in Fig. 4). The leptons produced in the decays of $Z$s at high rapidity are much more likely to fail the lepton acceptance cuts, which shaves off the high rapidity tail in the background distributions. As a result, the signal and background rapidity distributions become similar, but not identical. It is therefore worth asking how much one can gain by utilizing the residual rapidity differences observed in the figure.

To this end, in Fig. 5 we compare the ROC curves obtained from $KD$ with (blue lines) and without (red lines) PDF information included. In the absence of the lepton acceptance cuts (dashed lines), the difference between the ROC curves for the two processes is quite significant, as one might have guessed from Fig. 4. However, after the cuts (solid lines), the curves become quite similar and the advantage of using $KD$ with PDFs (Eq. (5)) with respect to using $KD$ without PDFs (Eq. (6)) can be quantified as being at the percent level.

## VI. SIGNAL-BACKGROUND SEPARATION FOR NON-SM SIGNALS

We showed the utility of the MEM, and in particular a tool like MEKD, for distinguishing the SM Higgs from the SM irreducible background. However, in general, the efficacy of the MEM in separating an arbitrary resonance from the background may depend on the spin and CP properties of the new state one is searching for. To illustrate this

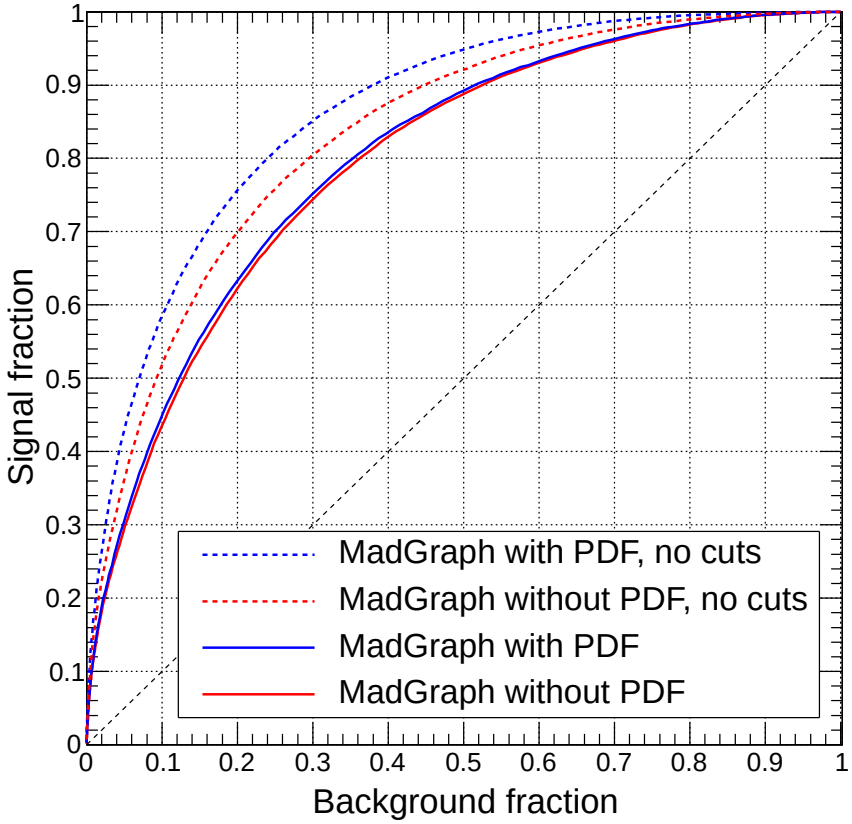


FIG. 5. Impact of parton distribution functions on ROC curves. The red curves are based on $KD(H;ZZ)$ from Eq. (6) and do not account for the longitudinal boost of the event, while the blue curves are based on $KD(H;ZZ)$ from Eq. (5) and include the effect from the parton distribution functions. Solid (dashed) lines are obtained from event samples with (without) the lepton acceptance cuts.

and to quantify the importance of this effect for several cases of interest, in Fig. 6 we show ROC curves indicating the ability of the MEM $KD$ to separate signal from background for three potential signals: SM Higgs boson ($J^{CP} = 0^+$), CP-odd scalar boson ($J^{CP} = 0^-$), and a massive graviton ($J^{CP} = 2^+_m$) in each of the three possible flavor states. We construct kinematic discriminants $KD(0^+;ZZ)$, $KD(0^-;ZZ)$, and $KD(2^+_m;ZZ)$ and apply all of them for each of the signal spin/parity samples.

There are three important lessons that one can derive from Fig. 6:

- The optimal separation between signal and background is achieved only when we use a kinematic discriminant $KD$ constructed with the correct signal hypothesis.

- However, the difference between the three discriminants is not dramatic. This is easy to understand since all three signal models assume, by construction, that the new resonances decay to $Z$ bosons, while the background has a fair amount of the $Z\gamma^*$ and even some $\gamma^*\gamma^*$ intermediate states. As was discussed in Sec. II (Fig. 1), the $m_{Z2}$ observable carries a lot of weight in the overall discrimination power of $KD(X;ZZ)$, which makes all three signals fairly alike as far as their separation from the background is concerned.

- There are differences between the ROC curves for the $e^+e^-\mu^+\mu^-$ final state and the SF final states for $0^-$ and $2^+_m$ signals. This suggests that, compared with the SM Higgs boson, the interference effects may play a more important role when the $0^-$ and $2^+_m$ hypotheses are considered. This is discussed further in the next section.

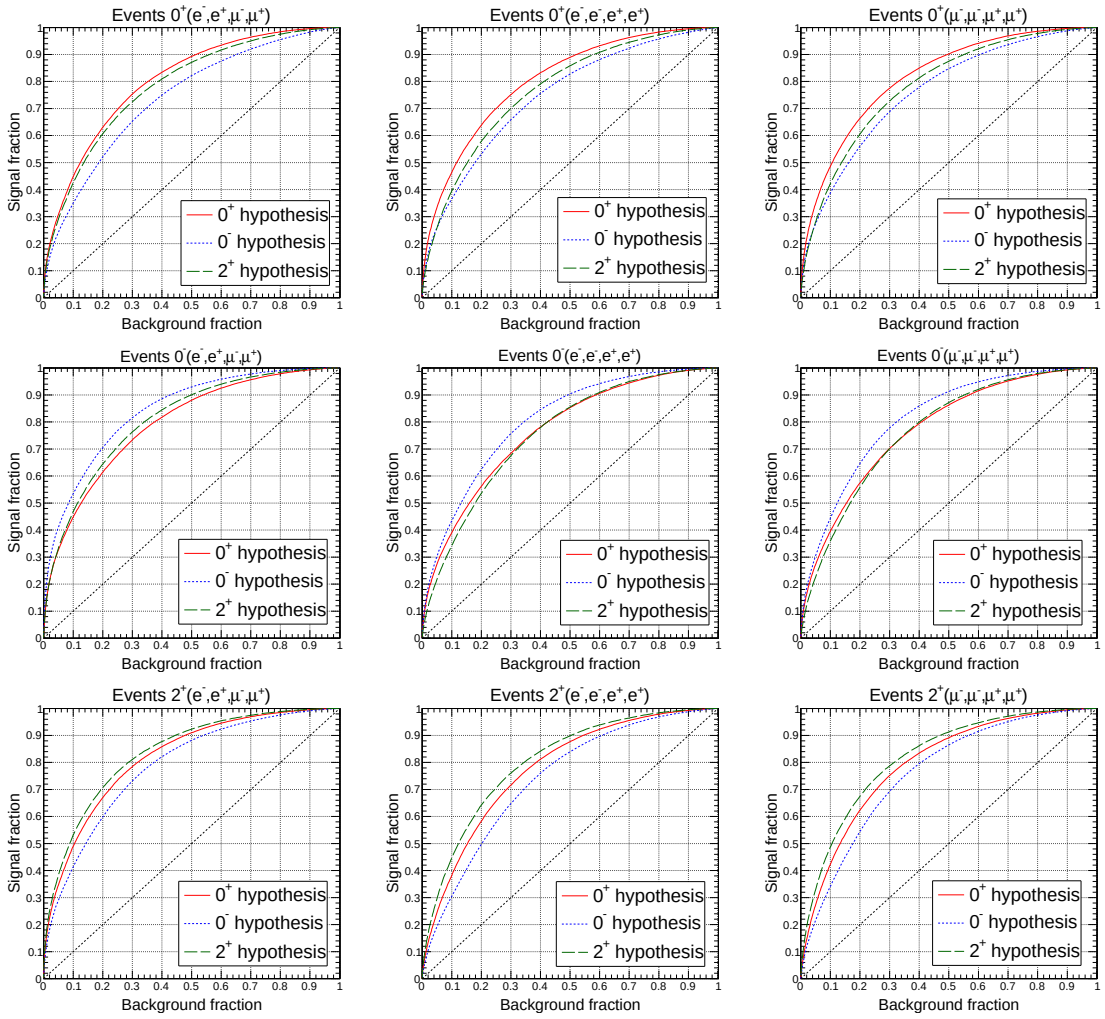


FIG. 6. ROC curves (as defined in Subsection II C) describing the separation between signal and background using MEKD where the signal is SM Higgs (top row), CP odd Higgs (middle row) or graviton (bottom row). The final states considered are $e^+e^-\mu^+\mu^-$ (left column), $e^+e^-e^+e^-$ (middle column), and $\mu^+\mu^-\mu^+\mu^-$ (right column).

## VII. SPIN AND PARITY DISCRIMINATION

An important and well-studied use of the golden channel is for determining the spin and parity of a putative Higgs boson. As we show below, the use of the exact matrix element for constructing kinematic discriminants plays a crucial role in achieving the best separation between alternative signal hypotheses. As an example, we consider two alternative signal models: a pseudoscalar boson ($J^{CP} = 0^-$) and a massive graviton, which is, of course, a spin two boson, ($J^{CP} = 2^+_m$). The couplings for the CP-odd scalar and the massive graviton are defined in Sec. III. To generate SM Higgs boson, pseudoscalar, and spin massive gravitons events, we use MadGraph. The kinematic cuts on the leptons are the same as described in Sec. II B. We then use ROC curves for the kinematic discriminant $KD(J^{CP}; H_{SM})$ to quantify the differences in kinematics of the four lepton system for the $J^{CP}$ boson and the SM Higgs boson ($H_{SM}$), as shown in Fig. 7.

There are three important conclusions to be drawn from this figure. First, one can see that the separation between the $0^-$ boson and $H_{SM}$ is more pronounced in comparison with the $2^+_m$ boson case. This indicates that one should be able to tell the difference between the $0^-$ boson and $H_{SM}$ sooner than between the $2^+_m$ boson and $H_{SM}$. Second, there is a significant difference between the SF ($4e$ and $4\mu$) and DF ($2e2\mu$) four lepton final states. This is a clear indicator that the allowed permutations of identical leptons and the associated interference in the SF events play a significant role. The detriment to sensitivity in neglecting such effects in constructing $KD$ will be discussed below. Third, for the $2^+_m$ boson, there is more expected separation with the SM Higgs for the SF final state as opposed to the DF final state, while for the $0^-$ boson case the opposite is true. Consequently, one should expect that the proper treatment of

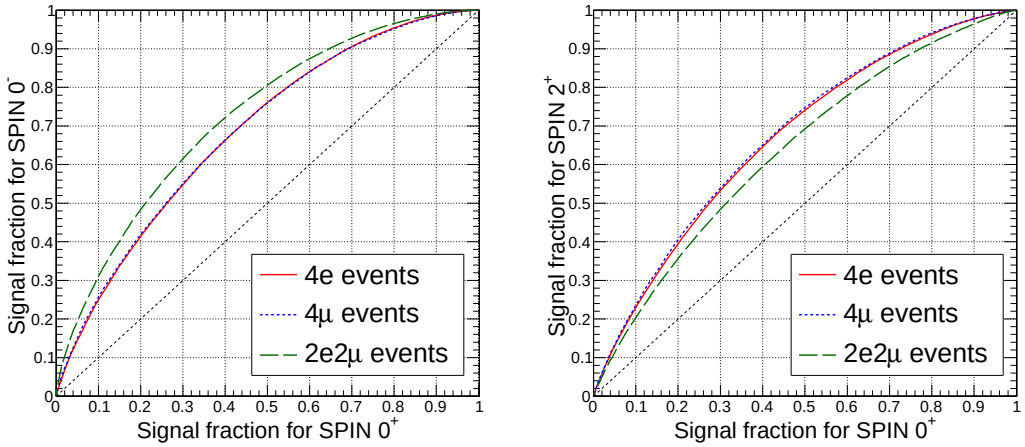


FIG. 7. ROC curves, shown for all three final state flavors ($4e$, $4\mu$, $2e2\mu$), display the separation of alternative signal hypotheses: (left) the pseudoscalar ($\mathrm{J}^{\mathrm{CP}} = 0^-$) vs. the SM Higgs boson ($0^+$); (right) the massive graviton ($\mathrm{J}^{\mathrm{CP}} = 2^+_m$) vs. the SM Higgs boson ($0^+$).

permutations/interference in the construction of $KD$ should lead to a greater ability to separate the $2^+_m$ boson from the SM Higgs boson in comparison with the $0^-$ boson case.

In order to further elucidate the role of permutations and interference effects, we proceed with a more detailed analysis of the four muon final state, $(\mu_1^-\mu_1^+)(\mu_2^-\ \mu_2^+)$. Here, the first dimuon pair, $(\mu_1^-\mu_1^+)$, is formed from the pair of opposite-charge muons whose invariant mass is closest to the $Z$ boson mass. We calculate three "matrix elements" for this final state as follows:

1. The complete leading order matrix element squared, $|\mathcal{M}_{4\mu}|^2$, with all permutations of identical leptons and associated interference included. The choice of how one pairs muons in this case does not matter; the full matrix element does not depend on how a human wants to group the final state leptons.

2. The "symmetrized" matrix element squared $|\mathcal{M}_{2e2\mu}|^2_{\mathrm{sym}}$ that takes into account permutations of identical leptons, but ignores the associated interference effects:

$$|\mathcal{M}_{2e2\mu}|^2_{\mathrm{sym}} = \left|\,\mathcal{M}_{2e2\mu}(\,(\mu_1^-\mu_1^+)_e\,(\mu_2^-\mu_2^+)_\mu\,)\,\right|^2 + \left|\,\mathcal{M}_{2e2\mu}(\,(\mu_1^-\mu_2^+)_e\,(\mu_2^-\mu_1^+)_\mu\,)\,\right|^2, \tag{18}$$

   where the first pair, marked by a subscript $e$, is treated as if it were a pair of electrons.

3. The $2e2\mu$ matrix element squared without symmetrization, $|\mathcal{M}_{2e2\mu}|^2$, that ignores both permutations of identical leptons and the associated interference effects:

$$|\mathcal{M}_{2e2\mu}|^2 = \left|\,\mathcal{M}_{2e2\mu}(\,(\mu_1^-\mu_1^+)_e\,(\mu_2^-\mu_2^+)_\mu\,)\,\right|^2, \tag{19}$$

   where the first pair, marked by a subscript $e$, is treated as if it were a pair of electrons.

We compare the results obtained using each of these three treatments of the SF final state in Figs. 8, 9, and 10. Fig. 8 and Fig. 9 compare the values of $KD(\mathrm{J}^{\mathrm{CP}};\,\mathrm{H}_{\mathrm{SM}})$. In Fig. 10 the effect is shown through ROC curves, corresponding to those shown in Fig. 7. These figures clearly show that including or ignoring permutations and interference has a significant impact on the value of the kinematic discriminant calculated and the separation power between alternative signal hypotheses. Comparing Fig. 8 and Fig. 9 (or the right and left plots in Fig. 10) shows unambiguously that the impact on the expected separation power between the $2^+_m$ boson and $\mathrm{H}_{\mathrm{SM}}$ is much larger than for the case of the $0^-$ boson versus $\mathrm{H}_{\mathrm{SM}}$.

To translate the observed differences in the ROC curves into the expected differences in our ability to tell apart different spin-parity hypotheses, we perform a simplified statistical analysis using MEKD-based discriminants. As a toy example, using CalcHEP, we first calculate the expected number of events (SM Higgs boson, $0^-$ pseudoscalar, $2^+_m$ massive graviton, and $ZZ$ background) for an integrated luminosity of 25 fb$^{-1}$ at 8 TeV, with the following lepton selection cuts applied: $p_T > 5$ GeV, $|\eta| < 2.5$, $m_{\ell^+\ell^-} > 12$ GeV, $120 < m_{4\ell} < 130$ GeV. The bosons have mass 125 GeV. The signal event count is scaled by K-factor 1.9 to match the Higgs boson cross sections used by the LHC

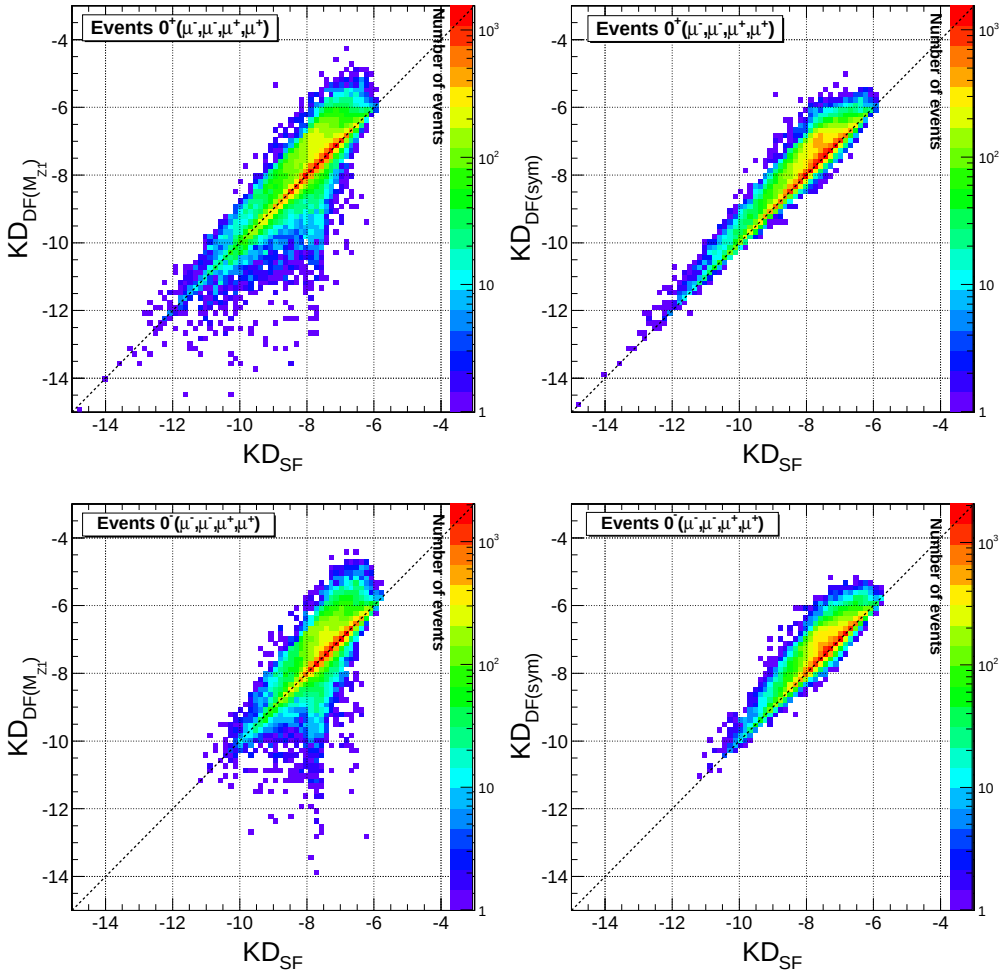


FIG. 8. Comparison of kinematic discriminants $KD(0^-;\,\mathrm{H_{SM}})$ for the four muon final states calculated with different levels of approximations. In all four plots, the $x$-axis shows the $KD$ calculated using the complete matrix element squared, $|\mathcal{M}_{4\mu}|^2$. In the plots on the left, the $y$-axis gives the $KD$ calculated using $|\mathcal{M}_{2e2\mu}|^2_{\mathrm{sym}}$, which takes into account permutations of identical leptons, but ignores the associated interference effects. In the plots on the right, the $y$-axis gives the $KD$ calculated using $|\mathcal{M}_{2e2\mu}|^2$, which ignores both permutations of identical leptons and the associated interference effects. The top plots are for SM Higgs signal events, while the bottom plots are for a pseudoscalar.

experiments. The $ZZ$ background event count is scaled up by a factor of 1.5 to approximately account for the NLO K-factor and presence of reducible $4\ell$ backgrounds, where one or more leptons are not prompt. This gives the following signal (background) event counts: 4.0(7.5) for the $4e$ final state, 3.9(7.0) for the $4\mu$ final state, and 8.9(15.5) for the $2e2\mu$ final state. We assume that the alternative signal hypotheses have the same cross sections as that of the SM Higgs boson and thus cannot be distinguished from it by using the information on the event yields in the four lepton mass distributions alone. We do not attempt to introduce any experimental event reconstruction/selection efficiencies. Thus the absolute numbers do not reflect accurately the expected separation power attainable by the LHC experiments; we are interested, rather, in the relative results when one does or does not include permutations/interference in the construction of kinematic discriminants. The statistical analysis is based on 2D *pdf*s for alternative signal+background hypotheses:

- $pdf(\,x, y\,|\,\mathrm{H_{SM}} + \mathrm{bkg}\,)$ for the standard model Higgs boson with background;
- $pdf(\,x, y\,|\,\mathrm{J^{CP}} + \mathrm{bkg}\,)$ for a signal of an alternative $\mathrm{J^{CP}}$ hypothesis with background,

where $x = KD(\mathrm{H_{SM}};\,ZZ)$ and $y = KD(\mathrm{J^{CP}};\,ZZ)$. We build these 2D *pdf*s using events generated with MadGraph. For background, we use the SM $q\bar{q} \to ZZ \to 4\ell$ process. Then we proceed with generation of pseudoexperiments, using the expected event yields and the 2D *pdf*s. The pseudoexperiments are generated for two different signal hypotheses,

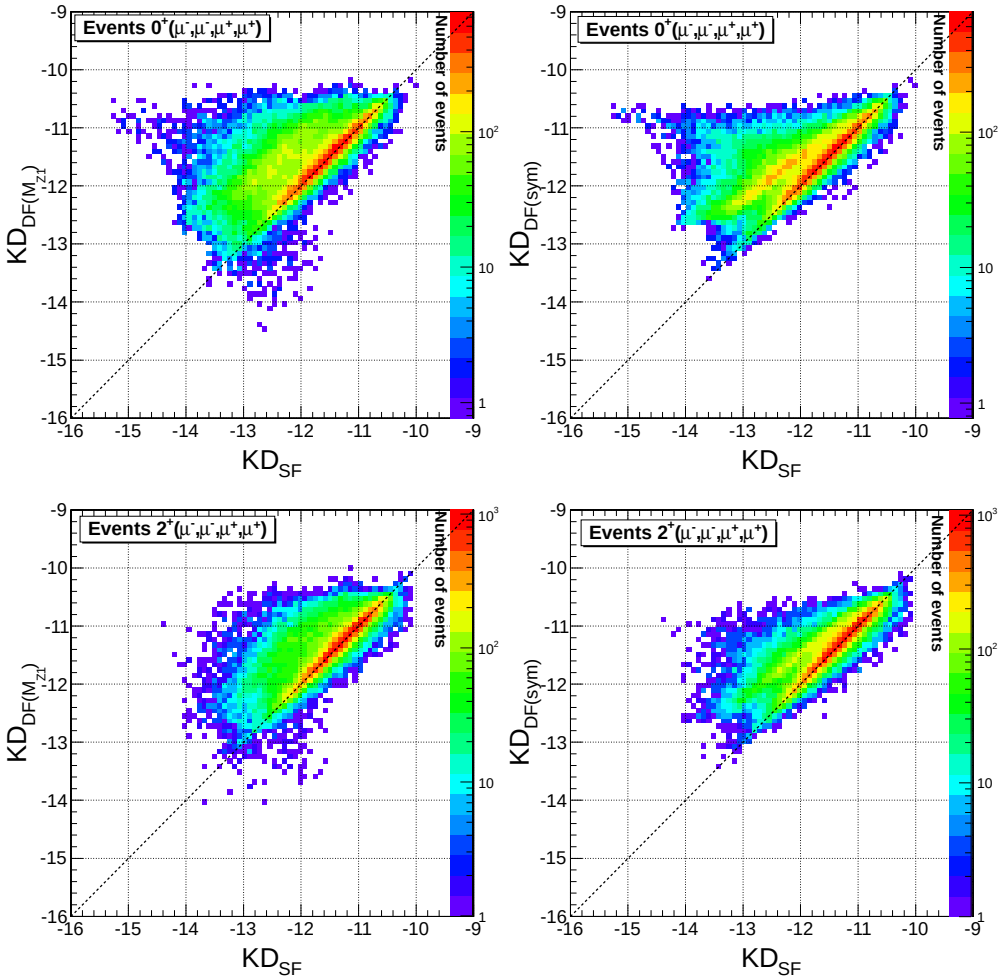


FIG. 9. Comparison of kinematic discriminants $KD(2^+_m;\,\mathrm{H_{SM}})$ for the four muon final states calculated with different levels of approximations. In all four plots, the $x$-axis shows the $KD$ calculated using the complete matrix element squared, $|\mathcal{M}_{4\mu}|^2$. In the plots on the left, the $y$-axis gives the $KD$ calculated using $|\mathcal{M}_{2e2\mu}|^2_{\mathrm{sym}}$, which accounts for permutations of identical leptons, but ignores the associated interference effects. In the plots on the right, the $y$-axis gives the $KD$ calculated using $|\mathcal{M}_{2e2\mu}|^2$, which ignores both permutations of identical leptons and the associated interference effects. The top plots are for the SM Higgs signal events, while the bottom plots are for a massive graviton.

the standard model Higgs boson and a boson with alternative $\mathrm{J^{CP}}$, in both cases assuming the presence of the $ZZ$ background. For each pseudoexperiment, we calculate as our test statistic, $q$, the negative log likelihood ratio:

$$q = -2\,\ln\frac{\mathcal{L}(\,\text{pseudoexperiment}\,|\,\mathrm{J^{CP}}+\text{bkg}\,)}{\mathcal{L}(\,\text{pseudoexperiment}\,|\,\mathrm{H_{SM}}+\text{bkg}\,)}. \tag{20}$$

Figure 11 shows the test statistic distributions for two alternative hypotheses: "massive graviton plus background" and "SM Higgs plus background", represented by open and filled histograms respectively. Figure 12 shows the test statistic distributions for alternative signal hypotheses: "pseudoscalar plus background" and "SM Higgs boson plus background". The three plots in each figure differ in how the $4e$ and $4\mu$ final states are treated in calculations of the matrix elements for signal, $\mathcal{M}_{\mathrm{H_{SM}}}$ and $\mathcal{M}_{\mathrm{J^{CP}}}$, and background, $\mathcal{M}_{ZZ}$, as follows:

- (left plot) complete leading order matrix element;
- (middle plot) permutations of identical leptons in $4e$ and $4\mu$ final states are accounted for, but the associated interference between diagrams is ignored;
- (right plot) both permutations and interference in $4e$ and $4\mu$ final states are ignored.

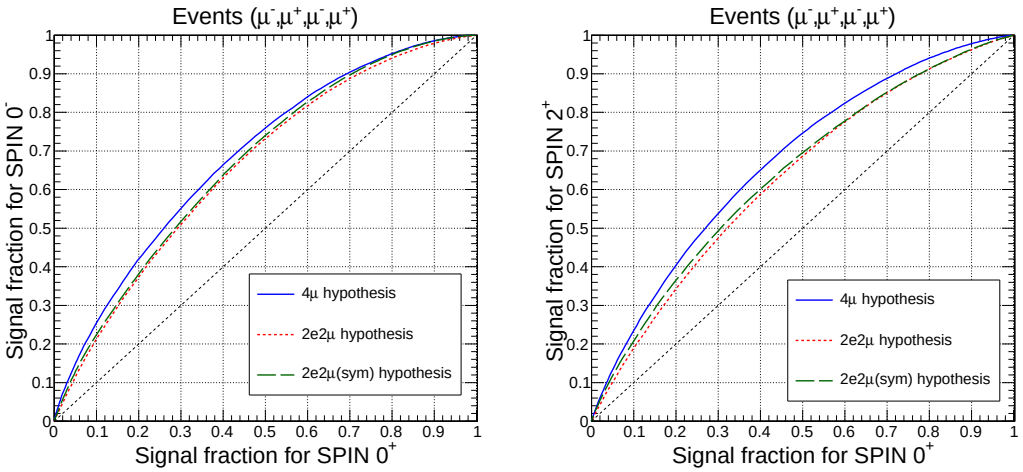


FIG. 10. ROC curves showing the separation of alternative signal hypotheses for the $\mu^+\mu^-\mu^+\mu^-$ final state: (left) the pseudoscalar ($J^{CP} = 0^-$) vs. the SM Higgs boson ($0^+$); (right) the massive graviton ($J^{CP} = 2^+_m$) vs. the SM Higgs boson ($0^+$). The solid blue curves are for $KD$s that use the full expressions for the squared matrix element for the four muon final state. The green dashed curves are for $KD$s that take into account permutations of identical leptons, but ignore the associated interference effects. The red dotted curves are for $KD$s that ignore both permutations of identical leptons and the associated interference effects.

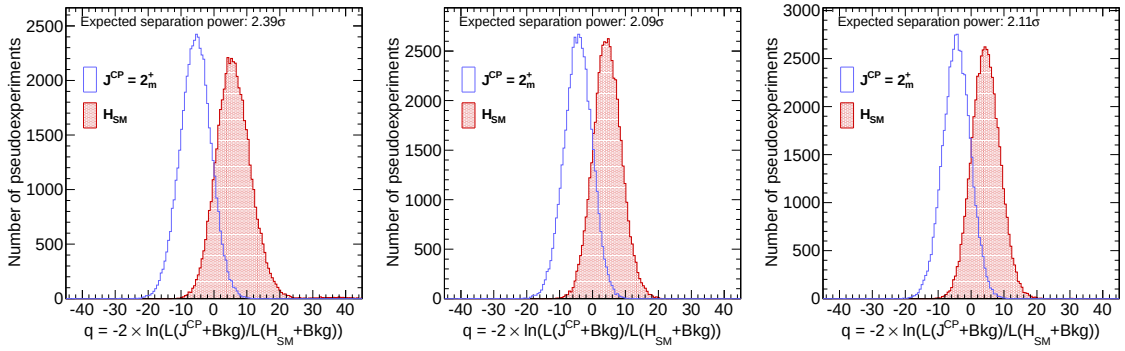


FIG. 11. Test statistic distributions for the two alternative hypotheses: "massive graviton plus background" and "SM Higgs boson plus background", open and filled histograms, respectively. The three plots differ in how the $4e$ and $4\mu$ final states are treated in calculations of the matrix elements: (left) complete leading order matrix element; (middle) permutations of identical leptons in $4e$ and $4\mu$ final states are accounted for, but the associated interference between diagrams is ignored; (right) both permutations and interference in $4e$ and $4\mu$ final states are ignored. The toy model used for generating pseudoexperiments is described in the text. The projected hypotheses separations are stated on the plots.

For the case of the massive graviton, there is about a 15% increase in sensitivity associated with the correct treatment of the SF four lepton final states. The difference is large and may become a decisive factor in the ability of ATLAS and CMS experiments to distinguish between spin zero and spin two bosons with the data of the 2011+2012 LHC run. As expected for the pseudoscalar case, the gain from the correct treatment of the SF final states is smaller, about 3%.

## VIII. SUMMARY AND OUTLOOK

We have shown that matrix element analyses improve the extent to which various Higgs-like signals can be discriminated from the background and allow for the measurement of the spin and parity properties of the Higgs-like boson in the $X \to ZZ^* \to 4\ell$ channel. We have demonstrated the importance of using the full matrix element including permutations of identical leptons and the associated interference terms for the SF four lepton final state. The proper treatment of these effects enhances our ability to distinguish between different spin and parity signal hypotheses. A

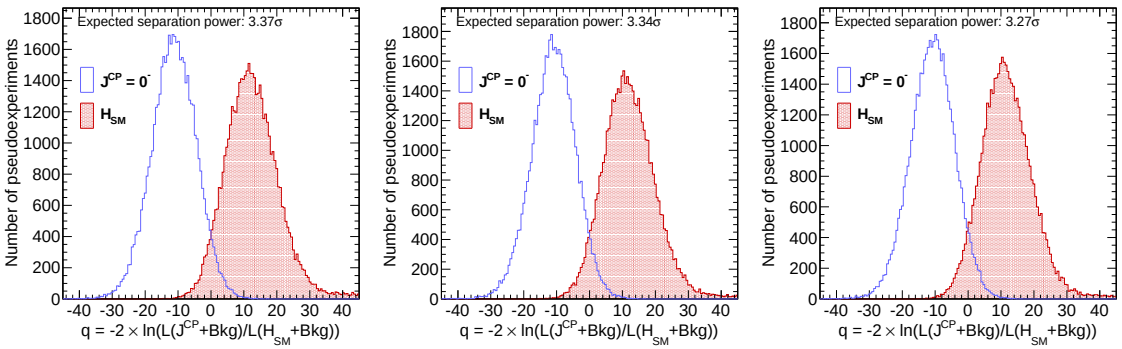


FIG. 12. Test statistic distributions for the two alternative hypotheses: "pseudoscalar plus background" and "SM Higgs boson plus background", represented by open and filled histograms, respectively. The three plots differ in how the $4e$ and $4\mu$ final states are treated in calculations of the matrix elements: (left) complete leading order matrix element; (middle) permutations of identical leptons in $4e$ and $4\mu$ final states are accounted for, but the associated interference between diagrams is ignored; (right) both permutations and interference in $4e$ and $4\mu$ final states are ignored. The toy model used for generating pseudoexperiments is described in the text. The projected hypotheses separations are stated on the plots.

gain in sensitivity as large as 15% can be expected for the case of SM Higgs vs. massive graviton hypothesis separation.

As the ATLAS and CMS experiments move toward precision studies of the properties of the observed boson, the kinematic discriminants will play larger and larger roles. Thus, the demand will grow for automated tools allowing for calculations of matrix element-based discriminants that most accurately capture all features of the underlying physics of the different signal and background processes involved.

The studies presented have been carried out with the MEKD code, which is now publicly available. The user of this code has the flexibility to construct signal matrix elements for an arbitrary set of allowed couplings for different spin zero and spin two resonances; the matrix element for the background process $q\bar{q} \to 4\ell$ is also a part of the package. The general couplings of a spin one boson as well as the ability to consider the final state with four leptons and a bremsstrahlung photon will be added shortly[73].

## ACKNOWLEDGMENTS

We thank J. Campbell, A. Gritsan, I. Low, J. Lykken, R. Vega-Morales, and C. Williams for useful discussions. J. Gainer and K. Matchev thank the Aspen Center for Physics (funded by NSF Grant #1066293) for hospitality during the completion of this work. M. Park is supported by the CERN-Korea fellowship through the National Research Foundation of Korea. Work supported in part by U.S. Department of Energy Grant DE-FG02-97ER41029 and NSF Grant 1007115.

## Appendix A: Validations of MEKD against CalcHEP and NLOME

### 1. Comparison with CalcHEP

Following the same procedure as in Sec. III, we also created an independent code to compute $KD_{\rm CALC}$, where the matrix element is calculated by CalcHEP. As in Sec. III, the SM is implemented via FeynRules, which ensures that our $KD_{\rm MAD}$ and $KD_{\rm CALC}$ results are obtained with identical inputs for the SM parameters (masses, couplings, etc.). Since there are no functionality differences between MadGraph and CalcHEP, one would expect that $KD_{\rm MAD}$ and $KD_{\rm CALC}$ should be the same; therefore this provides a useful cross-check.

We perform such consistency checks on both SM Higgs signal and background samples, for DF as well as SF final states. The results are displayed in Fig. 13, which reveals that, as expected, $KD_{\rm MAD}$ and $KD_{\rm CALC}$ are in excellent agreement. Perfect correlation is also observed for the signal and background matrix elements as calculated by the two tools. This synchronization exercise serves a dual purpose: first, we are able to validate our code, and second, the level of agreement seen in Fig. 13 provides a benchmark for the other comparisons in this paper.

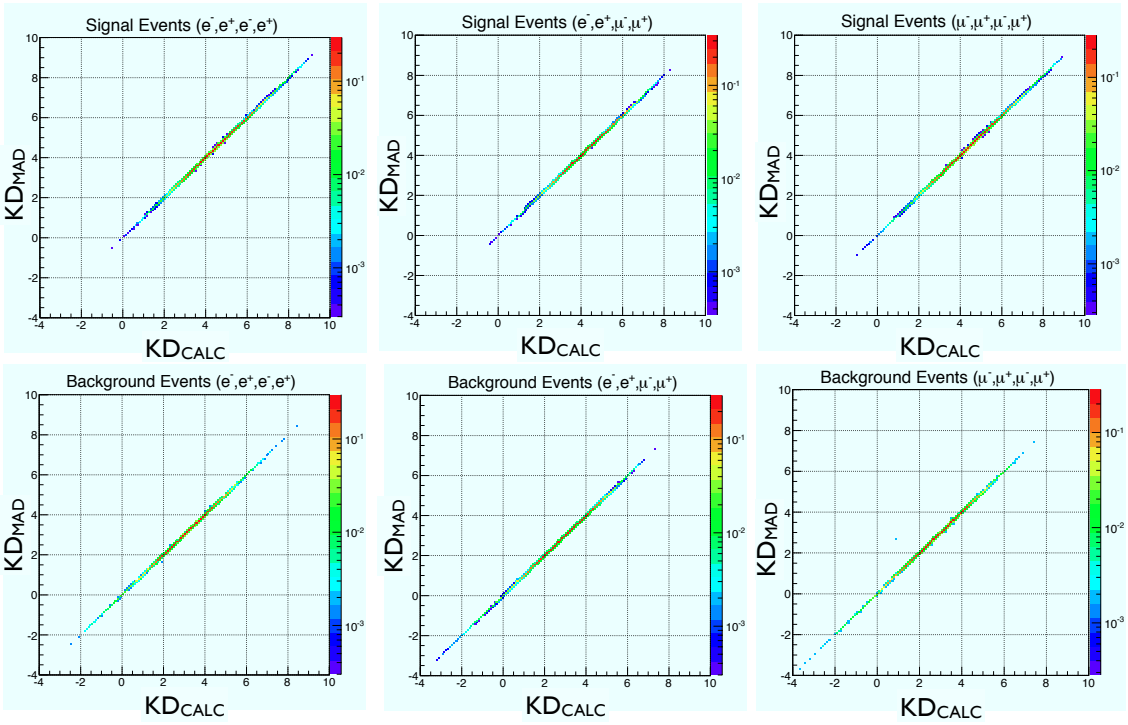


FIG. 13. Comparison of the kinematic discriminant, $KD_{\rm CALC}$, computed with CalcHEP, and the kinematic discriminant, $KD_{\rm MAD}$, computed by MadGraph, for SM Higgs signal events (top row) and background events (bottom row), using $4e$ events (left column), $4\mu$ events (right column), and $2e2\mu$ events (middle column).

### 2. Comparison with NLOME

The MCFM code[60] can be inverted to compute the matrix element weight $|\mathcal{M}|^2$ from a given final state kinematic configuration. The corresponding code, NLOME[61], is still under development. Here we use a beta version of NLOME to cross-check against our results from the previous two sections. We should mention that as an NLO tool, NLOME involves an integration over the unknown longitudinal momentum of the additional jets, which are recoiling against the $4\ell$ system. However, here we are using LO events, since we are interested in comparing the *leading order* machinery implemented in the different tools. Therefore, we removed the additional longitudinal momentum integration in NLOME and we are running the NLOME code in a purely LO mode.

The comparison between $KD_{\rm MAD}$ and $KD_{\rm NLOME}$ for DF $4\ell$ events is shown in Fig. 14. The two calculations for $2e2\mu$ final states are on equal footing and their results should agree. Indeed, this is what Fig. 14 shows: the level of agreement is excellent and comparable to what we observed earlier in Fig. 13.

## Appendix B: Notation and conventions

At leading order, events in the Higgs golden channel are described by 10 degrees of freedom[77]. Following[16,30], we can take them to be as follows:

- Three invariant mass parameters: $M_{4\ell}$, $M_{Z1}$ and $M_{Z2}$.
- The rapidity $y_{ZZ^*}$ of the event in the LAB frame, see Sec. V.
- Two angular variables defined in the CM frame of the whole event. These can be chosen to be the polar angle $\theta^*$ (measured from the beam axis) and the azimuthal angle $\Phi^*$ of the $Z_1$ system, as shown in Fig. 15.
- Two angular variables defined in the CM frame of the $Z_1$ system. These can be taken to be the azimuthal angle $\Phi_1$ and the polar angle $\theta_1$ (measured from the $Z_1$ direction in the Higgs CM frame) of the lepton $\ell_1^-$ produced in the $Z_1$ decay (refer to Fig. 15).

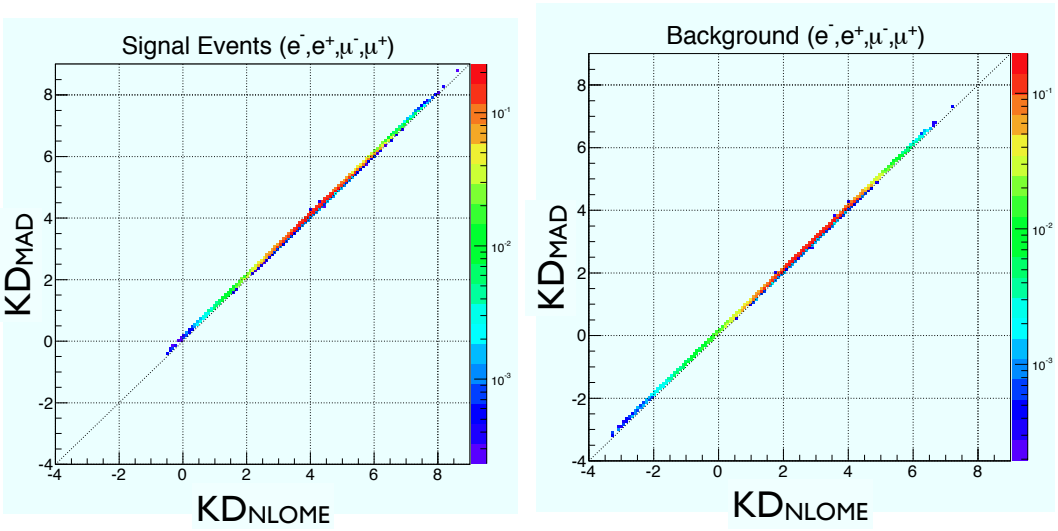


FIG. 14. Comparison of the kinematic discriminants $KD_{\rm NLOME}$ and $KD_{\rm MAD}$ for DF $2e2\mu$ events for SM Higgs signal (left plot) and background (right plot).

- Two angular variables defined in the CM frame of the $Z_2$ system. These can be taken to be the azimuthal angle $\Phi_2$ and the polar angle $\theta_2$ (measured from the $Z_2$ direction in the Higgs CM frame) of the lepton $\ell_2^-$ produced in the $Z_2$ decay. It is often convenient to trade the angle $\Phi_2$ for $\Phi \equiv \Phi_2 - \Phi_1$.

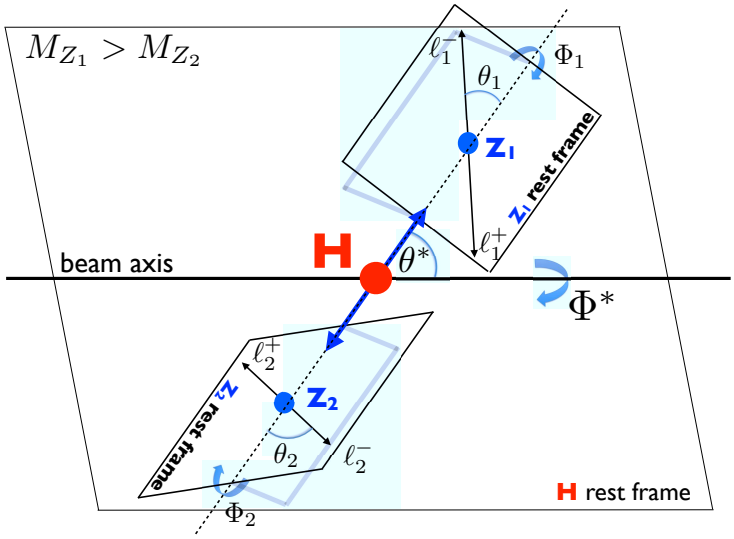


FIG. 15. Definition of the angular variables relevant to the $H \to ZZ^* \to 4\ell$ event topology.

## Appendix C: The Matrix Element Kinematic Discriminant package, MEKD

The computer code for calculating $KD_{\rm MAD}$ can be freely downloaded from[70]. The website also includes instructions and examples for installing the package and running the producer, which for completeness are also included here.

### 1. Description of the code

The Matrix Element Kinematic Discriminant, MEKD, package provides tools to calculate the leading order (LO) matrix elements for signal $gg \to X \to ZZ^* \to 4\ell$ and background $q\bar{q} \to ZZ^* \to 4\ell$ processes, and to build kinematic discriminants $KD$ that can be used for separation between these processes. The supported signal processes include the production of a scalar and a spin-2 resonance $X$ through gluon-gluon fusion and its decay into four leptons via two $Z$ gauge bosons, where the couplings of the scalar resonance to gauge bosons are kept general (parametrized). The MEKD package consists of two parts:

1. MEKD interface class (and the corresponding MadGraph libraries it depends on)

2. MEKD producer (macro defined in the `runKD_MAD.cc`)

The MEKD class is declared in `MEKD.h` and provides an interface to the methods to calculate the MEs and $KD$s for the chosen signal and background processes using the kinematic information about the four leptons in the final state. Detailed description of MEKD interface methods can be found at the dedicated MEKD class reference page at[70].

The macro `runKD_MAD.cc` is an executable that can run over the input sample of four lepton events and as an output produces a file with MEs and $KD$s for each of the input events. Its functionality is based on the MEKD interface class. The MEKD package provides the following functionalities:

1. Accepts as input the tabulated data file with the kinematic information of four leptons in the final state. The format of the input file is the following:

$$id_1\ id_2\ id_3\ id_4\ p_{1x}\ p_{1y}\ p_{1z}\ e_1\ p_{2x}\ p_{2y}\ p_{2z}\ e_2\ p_{3x}\ p_{3y}\ p_{3z}\ e_3\ p_{4x}\ p_{4y}\ p_{4z}\ e_4$$

   where $id_N$, $p_{Nx}$, $p_{Ny}$, $p_{Nz}$ and $e_N$ are the PDG id, spatial components and time component of the Nth lepton four momentum, respectively.

2. Allows the user to select the PDFs that should be taken into account in ME calculation.

3. Initializes the couplings of the resonance according to the user's signal selection.

4. Performs a purely transverse boost of each event to a reference frame where the transverse component of total momenta of the four lepton system is zero.

5. Feeds the boosted momenta of all four leptons to the ME calculator and computes MEs and the $KD$ for the given event.

6. Provides the output as the tabulated data file with the computed ME and $KD$ values. The format of the output file is the following:

$$|\mathcal{M}_{ZZ}|^2\ |\mathcal{M}_{XZZ}|^2\ KD$$

   where $|\mathcal{M}_{ZZ}|^2$, $|\mathcal{M}_{XZZ}|^2$ and $KD$ are the squared ME for the background process, the squared ME for the selected signal process and the kinematic discriminant $KD$, respectively.

7. Prints out the status of the code execution and the summary message at completion.

### 2. User instructions

#### *a. Requirements*

The latest version of the code can be downloaded and installed following the instructions at the MEKD web site:
`http://mekd.ihepa.ufl.edu/`
Compilation of the code requires an installed gcc compiler. GCC binary packages for multiple platform can be found here:
`http://gcc.gnu.org`

### b. *Setup of the* MEKD *code*

The package can be installed from the downloaded tarball by typing in a terminal window

```
tar xvf MEKD_Madgraph.tar
cd MEKD/macros
. setup.sh
```

The script will compile and link all necessary MEKD libraries/macros. One of the outputs is the main executable `runKD_MAD`. If ROOT framework is installed and the environment properly set, the code will be compiled with ROOT support.

### c. *Run the* MEKD *producer*

In a terminal window, type

```
./runKD_MAD [-f input_file] [-x x_resonance] [-p pdf_include] [-l log_file]
```

where the available options are described in Table I.

| | |
|---|---|
| `input_file` | name of the input `.dat` file (string, REQUIRED) |
| `x_resonance` | choice of the signal resonance (string, DEFAULT = 'SMHiggs')<br>Available options: SMHiggs, Higgs0M, Graviton2PM and Custom. |
| `pdf_include` | name of PDFs, not used if `pdf_include=''` (string, DEFAULT=`'CTEQ6L'`) |
| `log_file` | name of log file, no logging if `log_file=''` (string,DEFAULT=`''`) |

TABLE I. Options of the MEKD producer.

For example, to run the `.dat` file provided in the package, execute command:

```
./runKD_MAD -f DATA/Events/SIG_4l_30evt.dat
```

The user can define a resonance with custom couplings by specifying as the type of resonance "Custom" and by specifying manually the desired couplings in the file:

```
src/Cards/param_card.dat
```

Examples of files with couplings parameters can be found in template .dat files located in the same directory.

Options and details on input parameters can always be printed out as:

```
./runKD_MAD -h
```

### d. *Output from the* MEKD *producer*

To run the code with a user-provided input file, `yourInputFileName.dat`, evaluate

```
./runKD_MAD -f yourInputFileName.dat
```

and the output will be stored in the `.dat` file named

```
yourInputFileName_withDiscriminator.dat
```

It includes the MEs for selected signal and background, as well as the KD value.

### e. *Comparison of user MEKD results*

The results of a custom user code which uses the `MEKD.h` libraries can be compared to the results obtained by the `runKD_MAD.cc` macro. User code should be run on the input `.dat` files (SIG and BKG) which contain 30 events located here:

```
DATA/Events
```

The output files with MEKD results can be compared to the reference output files of the "`runKD_MAD`" macro located in the same directory.

* Corresponding author: gainer@phys.ufl.edu


[1] G. Aad *et al.* [ATLAS Collaboration], "Observation of a new particle in the search for the Standard Model Higgs boson with the ATLAS detector at the LHC," Phys. Lett. B **716**, 1 (2012) [arXiv:1207.7214 [hep-ex]].

[2] S. Chatrchyan *et al.* [CMS Collaboration], "Observation of a new boson at a mass of 125 GeV with the CMS experiment at the LHC," Phys. Lett. B **716**, 30 (2012) [arXiv:1207.7235 [hep-ex]].

[3] ATLAS Collaboration, "Observation of an excess of events in the search for the Standard Model Higgs boson in the gamma-gamma channel with the ATLAS detector", ATLAS-CONF-2012-091, `http://cdsweb.cern.ch/record/1460410`.

[4] CMS Collaboration, "Evidence for a new state decaying into two photons in the search for the standard model Higgs boson in pp collisions", CMS-PAS-HIG-12-015, `http://cdsweb.cern.ch/record/1460419?ln=en`.

[5] ATLAS Collaboration, "Observation and study of the Higgs boson candidate in the two photon decay channel with the ATLAS detector at the LHC", ATLAS-CONF-2012-168, `http://cdsweb.cern.ch/record/1499625`.

[6] ATLAS Collaboration, "Observation of an excess of events in the search for the Standard Model Higgs boson in the $H \to ZZ^* \to 4\ell$ channel with the ATLAS detector", ATLAS-CONF-2012-092, `http://cdsweb.cern.ch/record/1460411`.

[7] CMS Collaboration, "Evidence for a new state in the search for the standard model Higgs boson in the H to ZZ to 4 leptons channel in pp collisions at sqrt(s) = 7 and 8 TeV", CMS-PAS-HIG-12-016, `http://cdsweb.cern.ch/record/1460664?ln=en`.

[8] CMS Collaboration, "Updated results on the new boson discovered in the search for the standard model Higgs boson in the ZZ to 4 leptons channel in pp collisions at sqrt(s) = 7 and 8 TeV" CMS-PAS-HIG-12-041, `http://cdsweb.cern.ch/record/1494488?ln=en`.

[9] ATLAS Collaboration, "Updated results and measurements of properties of the new Higgs-like particle in the four lepton decay channel with the ATLAS detector", ATLAS-CONF-2012-169, `http://cdsweb.cern.ch/record/1499628`.

[10] L. D. Landau, "On the angular momentum of a two-photon system," Dokl. Akad. Nauk Ser. Fiz. **60**, 207 (1948).

[11] C.-N. Yang, "Selection Rules for the Dematerialization of a Particle Into Two Photons," Phys. Rev. **77**, 242 (1950).

[12] W. N. Cottingham and I. B. Whittingham, "Signals of Higgs sector CP violation in neutral Higgs boson decays," Phys. Rev. D **52**, 539 (1995).

[13] M. C. Kumar, P. Mathews, A. A. Pankov, N. Paver, V. Ravindran and A. V. Tsytrinov, "Spin-analysis of s-channel diphoton resonances at the LHC," Phys. Rev. D **84**, 115008 (2011) [arXiv:1108.3764 [hep-ph]].

[14] A. Alves, E. Ramirez Barreto, A. G. Dias, C. A. de S.Pires, F. S. Queiroz and P. S. Rodrigues da Silva, "Probing 3-3-1 Models in Diphoton Higgs Boson Decay," Phys. Rev. D **84**, 115004 (2011) [arXiv:1109.0238 [hep-ph]].

[15] J. Ellis and D. S. Hwang, "Does the 'Higgs' have Spin Zero?," arXiv:1202.6660 [hep-ph].

[16] S. Bolognesi, Y. Gao, A. V. Gritsan, K. Melnikov, M. Schulze, N. V. Tran and A. Whitbeck, "On the spin and parity of a single-produced resonance at the LHC," arXiv:1208.4018 [hep-ph].

[17] A. Alves, "Is the New Resonance Spin 0 or 2? Taking a Step Forward in the Higgs Boson Discovery," arXiv:1209.1037 [hep-ph].

[18] S. Y. Choi, M. M. Muhlleitner and P. M. Zerwas, "Theoretical Basis of Higgs-Spin Analysis in $H \to \gamma\gamma$ and $Z\gamma$ Decays," arXiv:1209.5268 [hep-ph].

[19] C. A. Nelson, "Correlation Between Decay Planes In Higgs Boson Decays Into W Pair (into Z Pair)," Phys. Rev. D **37**, 1220 (1988).

[20] A. Soni and R. M. Xu, "Probing CP violation via Higgs decays to four leptons," Phys. Rev. D **48**, 5259 (1993) [hep-ph/9301225].

[21] D. Chang, W. -Y. Keung and I. Phillips, "CP odd correlation in the decay of neutral Higgs boson into Z Z, W+ W-, or t anti-t," Phys. Rev. D **48**, 3225 (1993) [hep-ph/9303226].

[22] T. Arens and L. M. Sehgal, "Energy spectra and energy correlations in the decay $H \to ZZ \to \mu^+\mu^-\mu^+\mu^-$," Z. Phys. C **66**, 89 (1995) [hep-ph/9409396].

[23] S. Y. Choi, D. J. Miller, 2, M. M. Muhlleitner and P. M. Zerwas, "Identifying the Higgs spin and parity in decays to Z pairs," Phys. Lett. B **553**, 61 (2003) [hep-ph/0210077].

[24] C. P. Buszello, I. Fleck, P. Marquard and J. J. van der Bij, "Prospective analysis of spin- and CP-sensitive variables in $H \to ZZ \to l_1^+ l_1^- l_2^+ l_2^-$ at the LHC," Eur. Phys. J. C **32**, 209 (2004) [hep-ph/0212396].

[25] S. Schalla, "Study on the Measurement of the CP-Eigenstate of Higgs Bosons with the CMS experiment at the LHC," IEKP-KA-2004-14.

[26] R. M. Godbole, D. J. Miller, 2 and M. M. Muhlleitner, "Aspects of CP violation in the H ZZ coupling at the LHC," JHEP **0712**, 031 (2007) [arXiv:0708.0458 [hep-ph]].

[27] V. A. Kovalchuk, "Model-independent analysis of CP violation effects in decays of the Higgs boson into a pair of the W and Z bosons," J. Exp. Theor. Phys. **107**, 774 (2008).

[28] V. A. Kovalchuk, "Angular correlations and CP asymmetries in the decay $\Phi \to ZZ \to 4$ fermions," Prob. Atomic Sci. Technol. **2009N3**, 3 (2009).

[29] Q.-H. Cao, C. B. Jackson, W.-Y. Keung, I. Low and J. Shu, "The Higgs Mechanism and Loop-induced Decays of a Scalar into Two Z Bosons," Phys. Rev. D **81**, 015010 (2010) [arXiv:0911.3398 [hep-ph]].

[30] Y. Gao, A. V. Gritsan, Z. Guo, K. Melnikov, M. Schulze and N. V. Tran, "Spin determination of single-produced resonances at hadron colliders," Phys. Rev. D **81**, 075022 (2010) [arXiv:1001.3396 [hep-ph]].

[31] A. De Rujula, J. Lykken, M. Pierini, C. Rogan and M. Spiropulu, "Higgs look-alikes at the LHC," Phys. Rev. D **82**, 013003 (2010) [arXiv:1001.5300 [hep-ph]].

[32] C. Englert, C. Hackstein and M. Spannowsky, "Measuring spin and CP from semi-hadronic ZZ decays using jet substructure," Phys. Rev. D **82**, 114024 (2010) [arXiv:1010.0676 [hep-ph]].

[33] U. De Sanctis, M. Fabbrichesi and A. Tonero, "Telling the spin of the 'Higgs boson' at the LHC," Phys. Rev. D **84**, 015013 (2011) [arXiv:1103.1973 [hep-ph]].

[34] R. Boughezal, T. J. LeCompte and F. Petriello, "Single-variable asymmetries for measuring the 'Higgs' boson spin and CP properties," arXiv:1208.4311 [hep-ph].

[35] D. Stolarski and R. Vega-Morales, "Directly Measuring the Tensor Structure of the Scalar Coupling to Gauge Bosons," arXiv:1208.4840 [hep-ph].

[36] B. A. Kniehl, "The Higgs Boson Decay $h \to Z$ G G," Phys. Lett. B **244**, 537 (1990).

[37] B. A. Kniehl and O. L. Veretin, "Low-mass Higgs decays to four leptons at one loop and beyond," Phys. Rev. D **86**, 053007 (2012) [arXiv:1206.7110 [hep-ph]].

[38] C. Englert, M. Spannowsky and M. Takeuchi, "Measuring Higgs CP and couplings with hadronic event shapes," JHEP **1206**, 108 (2012) [arXiv:1203.5788 [hep-ph]].

[39] J. Moffat, "Identification of the 125 GeV Resonance as a Pseudoscalar Quarkonium Meson," arXiv:1207.6015 [hep-ph].

[40] B. Coleppa, K. Kumar and H. E. Logan, "Can the 126 GeV boson be a pseudoscalar?," arXiv:1208.2692 [hep-ph].

[41] P. Cea, "Comment on the evidence of the Higgs boson at LHC," arXiv:1209.3106 [hep-ph].

[42] J. Kumar, A. Rajaraman and D. Yaylali, "Spin Determination for Fermiophobic Bosons," arXiv:1209.5432 [hep-ph].

[43] J. S. Gainer, K. Kumar, I. Low and R. Vega-Morales, "Improving the sensitivity of Higgs boson searches in the golden channel," JHEP **1111**, 027 (2011) [arXiv:1108.2274 [hep-ph]].

[44] P. C. Bhat, "Multivariate Analysis Methods in Particle Physics," Ann. Rev. Nucl. Part. Sci. **61**, 281 (2011).

[45] J. M. Campbell, W. T. Giele and C. Williams, "The Matrix Element Method at Next-to-Leading Order," arXiv:1204.4424 [hep-ph].

[46] J. M. Campbell, W. T. Giele and C. Williams, "Extending the Matrix Element Method to Next-to-Leading Order," arXiv:1205.3434 [hep-ph].

[47] Y. Chen, N. Tran and R. Vega-Morales, "Scrutinizing the Higgs Signal and Background in the $2e2\mu$ Golden Channel," arXiv:1211.1959 [hep-ph].

[48] K. Hagiwara, R. D. Peccei, D. Zeppenfeld and K. Hikasa, "Probing the Weak Boson Sector in $e^+e^- \to W^+W^-$," Nucl. Phys. B **282**, 253 (1987).

[49] M. J. Duncan, G. L. Kane and W. W. Repko, "W W Physics at Future Colliders," Nucl. Phys. B **272**, 517 (1986).

[50] S. Ask, N. D. Christensen, C. Duhr, C. Grojean, S. Hoeche, K. Matchev, O. Mattelaer and S. Mrenna *et al.*, "From Lagrangians to Events: Computer Tutorial at the MC4BSM-2012 Workshop," arXiv:1209.0297 [hep-ph].

[51] N. D. Christensen and C. Duhr, "FeynRules - Feynman rules made easy," Comput. Phys. Commun. **180**, 1614 (2009) [arXiv:0806.4194 [hep-ph]].

[52] A. Semenov, "LanHEP: A Package for the automatic generation of Feynman rules in field theory. Version 3.0," Comput. Phys. Commun. **180**, 431 (2009) [arXiv:0805.0555 [hep-ph]].

[53] T. Stelzer and W. F. Long, "Automatic generation of tree level helicity amplitudes," Comput. Phys. Commun. **81**, 357 (1994) [hep-ph/9401258].

[54] J. Alwall, M. Herquet, F. Maltoni, O. Mattelaer and T. Stelzer, "MadGraph 5 : Going Beyond," JHEP **1106**, 128 (2011) [arXiv:1106.0522 [hep-ph]].

[55] A. Belyaev, N. D. Christensen and A. Pukhov, "CalcHEP 3.4 for collider physics within and beyond the Standard Model," arXiv:1207.6082 [hep-ph].

[56] A. Pukhov, E. Boos, M. Dubinin, V. Edneral, V. Ilyin, D. Kovalenko, A. Kryukov and V. Savrin *et al.*, "CompHEP: A Package for evaluation of Feynman diagrams and integration over multiparticle phase space," hep-ph/9908288.

[57] E. Boos, V. Bunichev, M. Dubinin, L. Dudko, V. Edneral, V. Ilyin, A. Kryukov and V. Savrin *et al.*, "CompHEP 4.5 Status Report," PoS ACAT **08**, 008 (2008) [arXiv:0901.4757 [hep-ph]].

[58] K. Kong, "TASI 2011: CalcHEP and PYTHIA Tutorials," arXiv:1208.0035 [hep-ph].

[59] Computer tutorials at the MC4BSM-2012 workshop, Cornell University, Ithaca NY, March 22-24, 2012, `http://www.phys.ufl.edu/~matchev/mc4bsm6/`.

[60] J. M. Campbell and R. K. Ellis, "MCFM for the Tevatron and the LHC," Nucl. Phys. Proc. Suppl. **205-206**, 10 (2010) [arXiv:1007.3492 [hep-ph]].

[61] C. Williams, "The Matrix Element Method at Next to Leading Order", talk given at the MC4BSM-6 workshop, Ithaca NY, March 22-24 2012.

[62] S. Chatrchyan *et al.* [CMS Collaboration], "Observation of Z decays to four leptons with the CMS detector at the LHC," arXiv:1210.3844 [hep-ex], CMS-PAS-SMP-12-009, *To be published in JHEP.*

[63] A. Denner, S. Heinemeyer, I. Puljak, D. Rebuzzi and M. Spira, "Standard Model Higgs-Boson Branching Ratios with Uncertainties," Eur. Phys. J. C **71**, 1753 (2011) [arXiv:1107.5909 [hep-ph]].

[64] J. Alwall, P. Demin, S. de Visscher, R. Frederix, M. Herquet, F. Maltoni, T. Plehn and D. L. Rainwater *et al.*, "MadGraph/MadEvent v4: The New Web Generation," JHEP **0709**, 028 (2007) [arXiv:0706.2334 [hep-ph]].

[65] J. Alwall, P. Artoisenet, S. de Visscher, C. Duhr, R. Frederix, M. Herquet and O. Mattelaer, "New Developments in MadGraph/MadEvent," AIP Conf. Proc. **1078**, 84 (2009) [arXiv:0809.2410 [hep-ph]].

[66] An elementary introduction to ROC curves is `http://en.wikipedia.org/wiki/ROC_curve`.

[67] C. Anastopoulos, N. Kerschen, and S. Paganis, "A 2D fit with background measurement constraints to boost the Higgs$\to$ZZ$^{(*)} \to 4\ell$ discovery potential at the LHC," Eur. Phys. J. C **71**, 1746 (2011).

[68] The code is available at `http://www.pha.jhu.edu/spin/`

[69] N. Tran, "Higgs properties at the LHC", talk given at the MCTP Higgs Symposium, April 18, 2012, http://www.umich.edu/~mctp/SciPrgPgs/events/2012/higgs/talks/ntran_120418_mctp.pdf.
[70] The $KD_{\rm MAD}$ code is available at http://mekd.ihepa.ufl.edu.
[71] L. Randall and R. Sundrum, "A Large mass hierarchy from a small extra dimension," Phys. Rev. Lett. **83**, 3370 (1999) [hep-ph/9905221].
[72] T. Han, J. D. Lykken and R. -J. Zhang, "On Kaluza-Klein states from large extra dimensions," Phys. Rev. D **59**, 105006 (1999) [hep-ph/9811350].
[73] P. Avery, D. Bourilkov, M. Chen, T. Cheng, A. Drozdetskiy, J. S. Gainer, A. Korytov, K. T. Matchev, P. Milenovic, G. Mitselmakher, M. Park, A. Rinkevicius, and M. Snowball, "Further precision studies of the Higgs boson decay channel $H \to ZZ \to 4\ell$ with MEKD " in preparation.
[74] T. Sjostrand, S. Mrenna and P. Z. Skands, "A Brief Introduction to PYTHIA 8.1," Comput. Phys. Commun. **178**, 852 (2008) [arXiv:0710.3820 [hep-ph]].
[75] Throughout this paper we shall use the convention that $Z$ stands for both on-shell and off-shell $Z$ bosons, as well as $\gamma^*$ when allowed, while $Z^*$ is used for either an off-shell $Z$ or for $\gamma^*$. We never make the approximation that a $Z$ is on-shell.
[76] We thank J. Campbell and C. Williams for making the beta version of the NLOME code available to us.
[77] There are four particles in the final state, whose momenta give $4 \times 3 = 12$ parameters, two of which are removed by transverse momentum conservation.